Targeting of Mammalian Glycans Enhances Phage Predation in the Gastrointestinal Tract

Sabrina I. Green[1], Carmen Gu Liu[1], Xue Yu[1], Shelley Gibson[2], Wilhem Salmen[1], Anubama Rajan[1], Hannah E. Carter[1], Justin R. Clark[1], Xuezheng Song[3], Robert F. Ramig[1], Barbara W. Trautner[4,5], Heidi B. Kaplan[6], Anthony W. Maresso[1#]

Address correspondence to Anthony Maresso, maresso@bcm.edu.

[1]Department of Molecular Virology and Microbiology, Baylor College of Medicine, Houston, TX, USA

[2]Department of Human Genetics, Baylor College of Medicine, Houston, TX, USA

[3]Department of Biochemistry, Emory Comprehensive Glycomics Core, Emory University School of Medicine, Atlanta, GA, USA.

[4]Michael E. Debakey Veterans Affairs Medical Center, Houston, TX, USA.

[5]Department of Medicine, Baylor College of Medicine, Houston, TX, USA.

[6]Department of Microbiology and Molecular Genetics, McGovern Medical School, University of Texas Health Science Center at Houston, Houston, Texas, USA.

Key Words

Phage therapy, *E. coli*, multidrug-resistance, bacteriophages, pathogen, pathobiont

Graphical Abstract

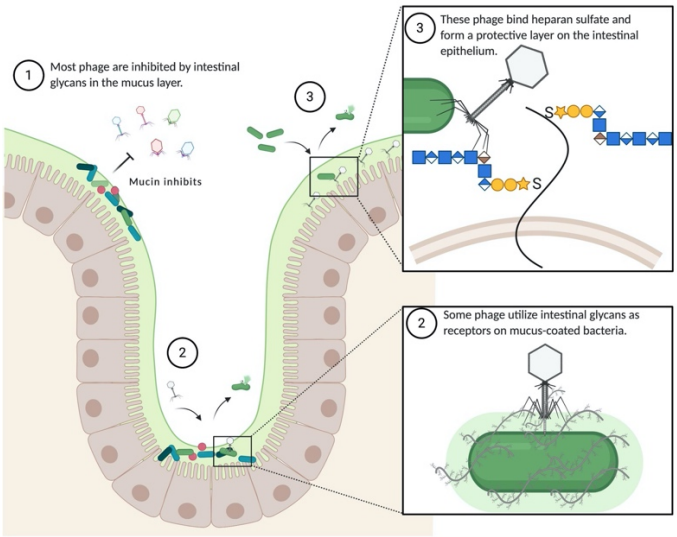

Model showing (1) mucins from the intestinal mucus layer inhibit phage infection, (2) phage ES17 can bind to mucin and utilize other intestinal glycans as a receptor to infect and kill mucus-coated bacteria, and (3) phages like ES17 can be utilized to coat the intestinal epithelium by binding heparan sulfate glycans to protect from invasive pathogen infection.

Abstract

The human mucosal surface consists of a eukaryotic epithelium, a prokaryotic microbiota, and a carbohydrate-rich interface that separates them. Bacteriophage parasitize the prokaryotes but are not known to associate with eukaryotic cells. In the gastrointestinal tract, the interaction of these two domains influences the health of the host, especially colonization with invasive pathobionts. Antibiotics may be used but they also kill protective commensals and lack the physio-chemical properties to be specifically and optimally active in this complex milieu. Here, we report a novel phage whose lytic cycle is enhanced in intestinal environments. The enhanced activity is encoded in its tail fiber gene, whose protein product binds human heparan sulfated proteoglycans and localizes the phage to the epithelial cell surface, thereby positioning

46 it near its bacterial host, a type of locational targeting mechanism. This finding offers the
47 prospect of developing epithelial-targeting phage to selectively remove invasive
48 pathobiont species from mucosal surfaces.
49
50 **Introduction**
51
52 The human mucosal surface is a diverse community comprised of bacteria, viruses,
53 fungi, and human epithelial, immune, and stem cells. The chemistry of the surface is
54 complex—commonly composed of proteins, lipids, nucleic acid, and small molecule
55 metabolites (Sansonetti, 2004; Nataro, 2005). The pH, ionic environment, and physio-
56 mechano properties also contribute to this dynamic surface. All of these factors
57 influence the biology, and, in turn, disease and treatment. Research over the last
58 decade has revealed the importance of mucosal homeostasis. Invasive pathobionts
59 may colonize, grow, and cause acute or chronic infections, some of which may become
60 systemic and life-threatening (Johnson JR, 2002; Russo and Johnson, 2003). The
61 bacterial composition of this intestinal community varies in association with human
62 illnesses such as cancer, diabetes, neurological illness, obesity, and cardiovascular
63 disease (De Martel *et al.*, 2012; Sampson and Mazmanian, 2015; Maruvada *et al.*,
64 2017; Vatanen *et al.*, 2018; Tang, Li and Hazen, 2019).
65
66 Antibiotics have revolutionized medicine. The meteoric rise of multidrug resistance
67 threatens a returns to pre-antibiotic days by 2050 (O'Neill, 2016). In addition, it is
68 increasingly recognized that antibiotics act as a commensal destroying napalm. The

69 antibiotics developed commercially have focused on inhibition of key processes
70 common to all bacterial species, for example, the inhibition of protein or cell wall
71 biosynthesis. Current antibiotics lack the specificity to selectively target a causative
72 pathobiont, which in the mucosal environment, might be the major driver of the disease
73 among the backdrop of hundreds of benign, even beneficial, symbionts. Moreover, the
74 core chemical backbones of antibiotics (e.g. β-lactam antibiotics) somewhat limit the
75 ability to develop new modified versions. Furthermore, these modifications improve
76 enzymatic activity (e.g. increase affinity or induced suicide inhibition) but has not
77 enhanced the drug's activity in the human mucosal environment. Mucosal-active,
78 targeted drugs that specifically control the bacterial composition of this complex
79 environment without perturbing ecological balance would promote the health of the
80 nasopharyngeal, lower respiratory, gastrointestinal, and urogenital epithelium.
81
82 The rise of multidrug resistance has precipitated the search for alternative antibacterial
83 approaches, including the use of bacteriophages (phages) which are bacterial viruses
84 used to treat infections. Although phage therapy has been used in Eastern Europe for
85 decades, only in the past few years has it been employed for compassionate use cases
86 in the U.S. and Europe and in clinical trials (Schooley *et al.*, 2017; Dedrick *et al.*, 2019;
87 Jault *et al.*, 2019). In theory, phage offer numerous advantages over antibiotics,
88 including that they can be specific towards a given species of bacteria resulting in
89 potential microbiome sparing, "generally regarded as safe" or GRAS attributes, allowing
90 them to be given in high doses, and diverse, as phage mixtures can be used to either
91 broaden the range or reduce the frequency of resistance or both (Loc-Carrillo and

92 Abedon, 2011; Grose and Casjens, 2014; Moye, Woolston and Sulakvelidze, 2018).
93 However, their greatest attribute has been speculated to be their abundance –
94 estimated to be 10^{31} on Planet Earth. The phage genosphere—all the collection of
95 genes and their unique biology—sometimes referred to as "viral dark matter", may
96 encode novel features that allow for enhanced lytic activity towards bacterial pathogens
97 (Youle, Haynes and Rohwer, 2012; Brum *et al.*, 2016; Terwilliger *et al.*, 2020).
98 Reasoning that this genosphere may include phage with unique phenotypes that
99 facilitate lytic activity against pathobionts at mucosal environments, we report here a
100 novel podovirus of the genus *Kuravirus* that infects pathogenic *E. coli* using positional
101 targeting to human heparan-sulfated proteoglycans.
102
103 **Results**
104
105 **The gastrointestinal tract is prohibitive to phage therapy**
106
107 *Escherichia coli* are gram-negative bacilli found in a variety of environments, including
108 the human intestinal microbiome, with > 90% of people colonized (Mitsuoka, Hayakawa
109 and Kimura, 1975). Although most strains are benign, *E. coli* is particularly troubling
110 because of its propensity to undergo horizontal transfer of genes encoding virulence
111 factors and antimicrobial resistance (Huang *et al.*, 2001; Antão, Wieler and Ewers,
112 2009; Price *et al.*, 2013; Mathers, Peirano and Pitout, 2015; Poole *et al.*, 2017). Thus,
113 several pathotypes have arisen that are associated with human disease. InPEC
114 (Intestinal pathogenic *E. coli*) are associated with diarrhea and gastroenteritis. ExPEC

115 (Extraintestinal pathogenic *E. coli*) are associated with systemic infections of the urinary
116 tract, brain, peritoneum, peripheral organs, blood, and in-dwelling devices, resulting in 9
117 million infections per year (Russo and Johnson, 2003; Colpan *et al.*, 2013; Poolman and
118 Wacker, 2016). The pandemic ExPEC sequence type 131 or ST131 possess a rare
119 combination of multidrug resistance and enhanced virulence (Pitout, 2012; Johnson *et*
120 *al.*, 2013; Banerjee and Johnson, 2014). These strains readily colonize the human
121 intestine, which can become a reservoir, prior to extraintestinal infection (Nicolas-
122 Chanoine, Bertrand and Madec, 2014). Previous studies reported that phage HP3, a
123 lytic myovirus isolated from environmental reservoirs of ExPEC, could reduce ST131
124 bacteremia and disease severity in murine models of infection (Green *et al.*, 2017a; Ma
125 *et al.*, 2018). Since the human gastrointestinal tract is the primary reservoir of ExPEC
126 ST131, we wondered if phage HP3 could act prophylactically to reduce or eliminate
127 ExPEC burden in the intestine. To test this, mice were orally gavaged with an ExPEC
128 ST131 clinical isolate then treated with phage or an antibiotic as illustrated in Figure 1A.
129 Untreated mice sustained stable bacterial colonization during the course of the
130 experiment (6 days) (Figure 1B). When phage HP3 were given to animals via water or a
131 daily gavage, the levels of ExPEC were indistinguishable from the untreated control at
132 the end of the experiment. However, no ExPEC was detected at any time point in the
133 antibiotic-treated group. Interestingly, phage HP3 was detected, and active, in the stool
134 of phage-treated mice, even on day 4, indicating the lack of ExPEC reduction was not
135 due to a lack of delivery to the intestinal environment or to inactivation of the phage
136 (Figure 1C). It should also be noted that despite having higher levels of phage upon
137 gavage during days 1-4, the phage was no more effective at removing ExPEC than

138 phage given in the water, suggesting that in this experiment there was no dose
139 dependent effect of phage. In addition, as much as 10^5 (PFU/g) phage were found in the
140 murine intestinal tissue (including cecum and colon) on day 6, the final day of the study,
141 yet there was little to no clearing of ExPEC compared to the untreated control in these
142 tissues (Figures 1D and 1E). Importantly, antibiotic treatment significantly reduced the
143 number of operational taxonomic units (OTUs) and diversity, as determined by the
144 Shannon diversity index, which takes into account species richness and distribution
145 (Figure 1Fi, ii, $p = 0.007$, $p = 0.009$). Also, a Principle component analysis (PCA) of beta
146 diversity demonstrated that mice in the antibiotic cohort clustered together and away
147 from the untreated and phage groups, suggesting antibiotics had a more profound effect
148 on the microbiome than did phage (Figure 1Fiii). Finally, we assessed phage killing in a
149 modified "cecal medium" or CM that is derived from the murine cecal contents and
150 designed to simulate the luminal complexity of the mammalian intestine (Figure 1G).
151 Whereas phage HP3 completely abolished ExPEC in LB (nearly a 9-log drop in levels
152 and no detectable live bacteria), and nearly abolished it in a slurry of fecal pellets taken
153 from the same murine host (~ 8-log drop in levels), there was little to no phage-based
154 killing in CM, despite recovering nearly 10^6-$10^{7.5}$ PFU/mL (Figures 1H and 1I) of phage.
155 The result was the same when the experiment was repeated anaerobically (data not
156 shown). These results mirrored those from the ExPEC colonization model and indicate

157 there is/are factor(s) present in the mammalian GI that inhibit this lytic phage.

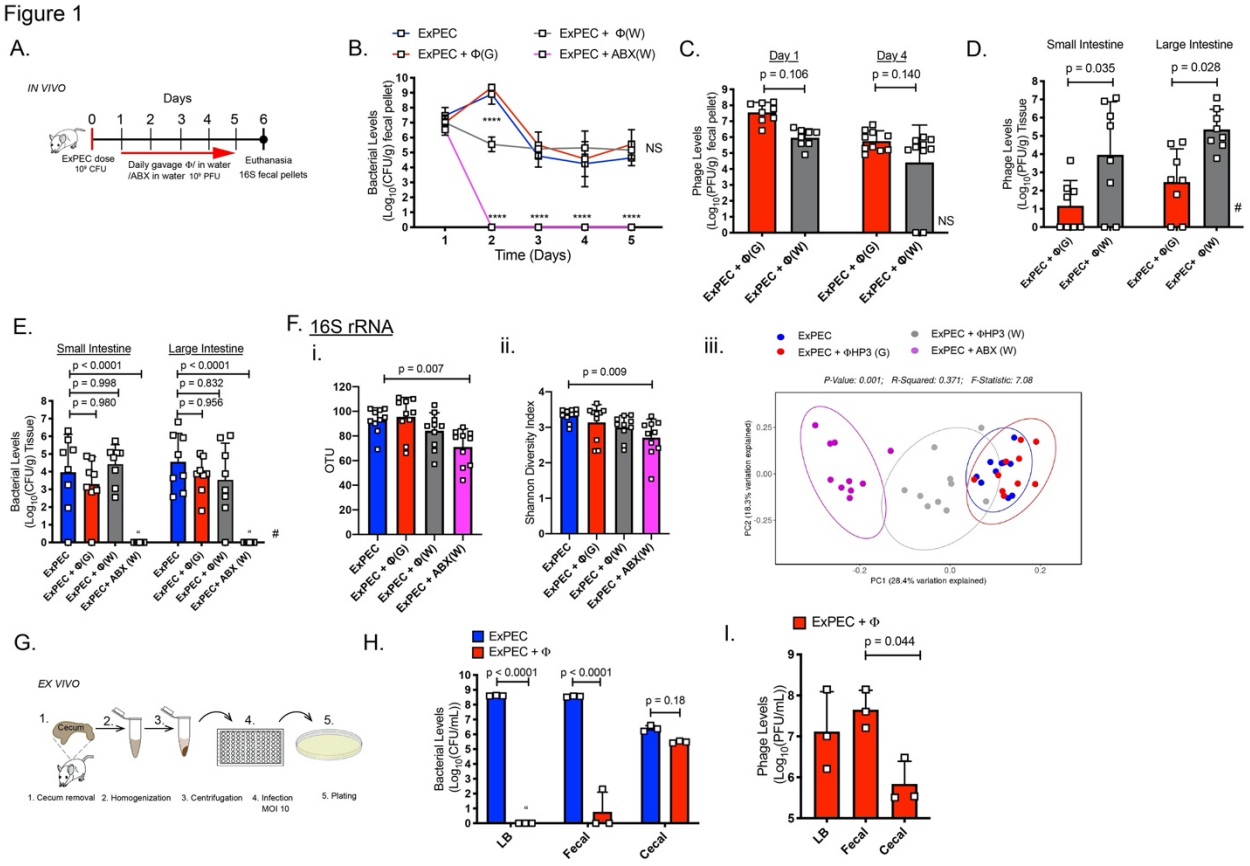

158

159 **Figure 1: The gastrointestinal tract is prohibitive to phage therapy**
160 (A) Mouse colonization diagram. (B) Intestinal (fecal) colonization of ExPEC (C) and phage HP3
161 levels. (D) Day 6 intestinal tissue HP3 levels and (E) ExPEC levels. (Fi) OTU from 16S rRNA
162 analysis of fecal pellets day 6. (Fii) Shannon diversity values (Fiii) PCA of beta diversity.
163 Symbols (squares) indicate individual mice, except in (B) squares indicate mean. Exp.
164 performed 1X. N=8-10 where N indicates individual mice. **** $p < 0.0001$, NS not significant," =
165 none detected, # missing values due to histological analysis of 2 mice/group. Mean, ±SD
166 shown. (G) Cecal medium (CM) development. (H) ExPEC levels after 4.5 hours growth and (I)
167 phage HP3 levels. Experiment performed 1X. Squares (N=3) indicate individual biological
168 replicates from independent cultures. Mean, ±SD shown.
169
170

171 **The inhibitory component is mucin**

172

173 We wished to understand the reasons phage HP3 was ineffective in this intestinal

174 microenvironment. Previously, we had shown that phage HP3 utilizes calcium for

175 efficient infection, suggesting the effect may be nutritionally-based (Ma *et al.*, 2018).
176 However, addition of calcium did not increase phage HP3 killing in CM (data not
177 shown). We next tested whether the inhibition might be related to the presence of live
178 bacterial microbiota in CM. However, ExPEC killing with phage was not enhanced with
179 removal of the microbiota with a broad range of antibiotics, including inhibitors of protein
180 synthesis, cell wall, and DNA synthesis (Figure S1i-iii – note that the antibiotics
181 efficiently killed a commensal, antibiotic-sensitive, *E. coli* that was spiked into the CM,
182 iv). Furthermore, the inhibitory effect was maintained when a related, and equally as
183 effective phage EC1 was used in the same experiment, thereby indicating the inhibitory
184 effect was not solely due something specific for phage HP3 (data not shown). Arriving at
185 no resolution as to what the inhibitory factor may be, we decided to test more drastic
186 treatments for their ability to restore phage killing in CM. First, the CM was heat-treated
187 (Figure 2Ai, HT CM). Interestingly, heat treatment led to greater than a 6-log
188 improvement in ExPEC killing by phage HP3 (Figure 2Aii, $p < 0.0001$). Similarly, when
189 CM was filter-treated (Figure 2Ai, FT CM), there was no detectable levels of ExPEC in
190 the medium after treatment with phage HP3 (Figure 2Aii), and, this observation was
191 extended to another phage showing inhibition in CM, EC1 (Figure S2A, $p < 0.0001$).
192 Thus, the inhibitory component was large (retained on 0.22 micron filter) and sensitive
193 to boiling.
194
195 We reasoned intestinal mucins might fit this profile due to their highly associative and
196 sticky properties (captured on a filter) and as proteins they would be sensitive to heat.
197 Mucins are extensively glycosylated proteins found throughout the gastrointestinal

198 system, which form a layer between the intestinal epithelial cells (IECs) and the
199 commensal or pathogenic microbiota (Johansson and Hansson, 2016). Also, they can
200 function as receptors for microbes (McGuckin *et al.*, 2011). To test whether mucins
201 were inhibiting bacterial killing by phage, we devised another method whereby CM was
202 separated via high speed centrifugation into soluble (S CM) and insoluble (INS CM)
203 forms (Figure 2Bi). We hypothesized that INS CM would contain mucin, since large
204 intestinal mucins are normally present in this portion, and be inhibitory to phage killing,
205 whereas the S CM would not have these properties (Carlstedt *et al.*, 1993). Indeed,
206 phage killing in unprocessed CM or INS CM was inhibited to a greater extent than in S
207 CM (Figure 2Bii). To more directly test the hypothesis that mucin was the inhibitory
208 factor, the mucolytic drug N-acetyl cysteine (NAC) was added to INS CM and porcine
209 gastric mucin (1.5 % m/v) added to S CM (Figure 2Bi-ii). Indeed, a 5-log reduction in
210 phage killing of ExPEC was observed in INS CM upon addition of NAC, which also
211 improved killing to that seen in S CM ($p < 0.0001$). Perhaps more compelling, the
212 addition of mucin to S CM abrogated bacterial killing by phage to levels originally
213 observed in CM alone (not significant $p = 0.970$). These results indicate that the inhibitor
214 of phage killing in cecal medium is intestinal mucin.

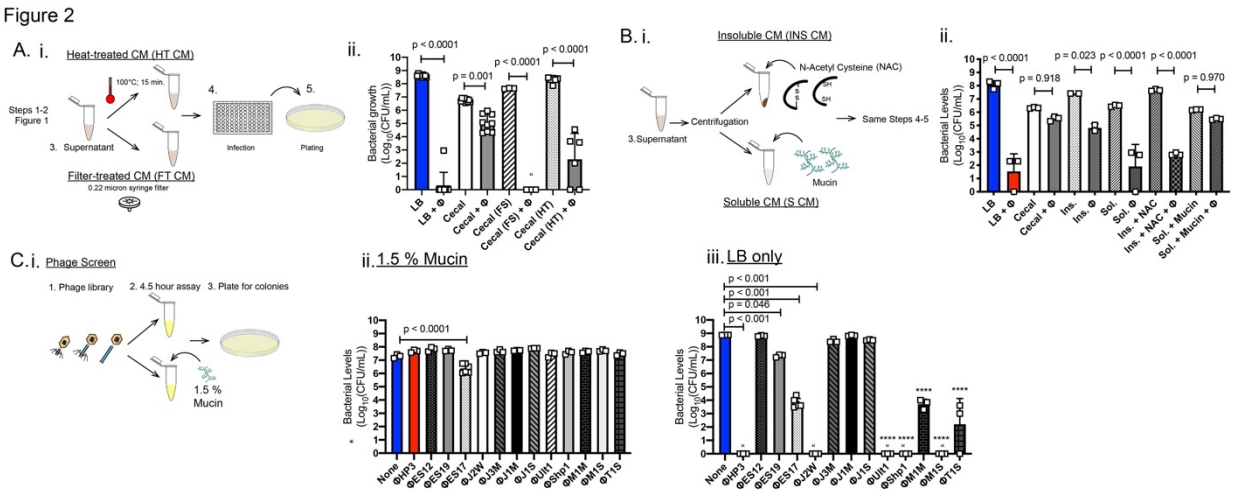

Figure 2: The inhibitory component is mucin. (Ai) CM was heat-treated (HT, 100°C) or filter treated (FT) prior to assay. (Aii) ExPEC levels in HT CM and FT CM. (Bi) CM was separated into pellet (insoluble), homogenized and treated with N-acetyl cysteine (NAC), or into supernatant (soluble) and mucin added. Following assay modified CM was plated for (Bii) ExPEC levels. (Ci) A screen of phage killing in mucin was performed using the phage in Table 1. (Cii) ExPEC levels in LB + 1.5% mucin. (Ciii) LB alone. N=3-6, **** $p < 0.0001$, " = none detected. Exp. performed 1X (B), 2X (A and C). Squares indicate individual biological replicates from independent cultures. Mean, ±SD shown.

Along these lines, *E. coli* is known to use mucins as a source of carbon (Chang *et al.*, 2004). We reasoned that a murine host colonized with ExPEC may see a bloom upon NAC treatment due to the drug liberating the mucins for bacterial consumption and thus serve as a system to test if the reduction in aggregated mucin would promote phage HP3's ability to kill ExPEC. Indeed, upon treatment with NAC for two weeks, ExPEC levels in the small intestine were increased and phage HP3 reduced ExPEC levels, 2.5 logs, in the small intestine (Figure S2Bi-ii). A similar trend was observed in the large intestine, but it was not substantial (<1 log reduction), though in both organ sections the data were not significant (Figure S2Biii). The less pronounced effect in the large intestine may be due to the thickness of mucus, and thus the lower likelihood for NAC to be effective at breaking up this mucus. Also, NAC's known to be rapidly absorbed in the

236 small intestinal tissue, thereby losing its effect in the more distal large intestine (Aruoma
237 *et al.*, 1989; Tsikas *et al.*, 1998).
238
239 **Discovery of a mucin-enhanced phage**
240
241 An estimated 10^{31} phages exist in nature. And the human gastrointestinal tract contains
242 a large diversity consisting of $>10^{10}$ phages many of which are just beginning to be
243 discovered (Shkoporov and Hill, 2019; Sausset *et al.*, 2020). Reasoning that human
244 sewage or the feces of animals may contain phage that have evolved to target their host
245 in high mucin environments, such as the intestinal tract, we screened our phage library
246 (Gibson *et al.*, 2019) and other phages (Table 1) recently isolated from these
247 environments for enhanced activity in LB containing 1.5% mucin (Figure 2C). This is the
248 same concentration that prevented phage HP3 activity in soluble cecal medium and was
249 shown to provide strong inhibition in LB for up to 8 hours (Figure S3A). Surprisingly,
250 only a single phage, designated phage ES17, significantly killed bacteria in the LB
251 mucin medium (Figure 2Cii, $p < 0.0001$, about 1-log improvement). Surprisingly, phage
252 ES17 was active in mucin despite being much less effective (> 3-logs) than phages
253 HP3, J2W, Ult1, Shp1, or M1S, which completely killed ExPEC to undetectable levels in
254 LB medium alone (Figure 2Ciii, LB). Consistent with these data, when the amount of
255 mucin was varied from 0 to 2% and phages HP3 and ES17 were compared for lytic
256 activity against ExPEC, phage HP3 was highly effective as the concentration of mucin
257 was lowered to below 0.5%, but completely inhibited above that level (Figure S3B).
258 However, phage ES17 was most effective at concentrations in which HP3 was inactive

259 (0.5 – 1% mucin) and least active at concentrations below or above this range. Taken
260 together, these data suggests that phage ES17 harbors unique properties that facilitate
261 its ability to efficiently be lytic in the presence of mucin.
262
263 **Phage ES17 is a rare C3 type phage whose activity is enhanced by mucin.**
264
265 We sought to understand the molecular mechanism of phage ES17's enhanced ability
266 to find and lyse its bacterial host in mucin. Phage ES17 was determined to be a dsDNA
267 virus of the order *Caudovirales*, family *Podoviridae* and genus *Kuravirus*. The genus
268 *Kuravirus* was named for the River Kura in Tbilisi, Georgia where the original phage of
269 this genus, PhiEco32, which shows close genetic similarity to ES17, was first isolated
270 (Figure S4A) (Savalia *et al.*, 2008). Kuravirus phages have similar morphological
271 characteristics (Ren *et al.*, 2019), including an elongated C3 type capsid, which is
272 considered a rare morphotype for phages (only 13% of tailed phages have elongated
273 heads) and short tail fibers (Ren *et al.*, 2019). Electron microscopy confirmed ES17 to
274 have these same morphological characteristics (capsid >100 nm – Figure 3A). Similar to
275 other phages of this genus, ES17 has a small genome size consisting of 75,007 bps
276 with 123 predicted ORFs (Figure 3B).
277
278 In order to determine why this phage is distinct from other phages that lack activity in
279 mucin-rich environments, we examined the ability of phages ES17 and HP3 to adsorb to
280 their *E. coli* hosts. Previous data had shown that 98% of HP3 was adsorbed in 10
281 minutes, whereas only 32% of ES17 was adsorbed in that time (Gibson *et al.*, 2019).

282 We wondered whether the addition of mucin could improve phage ES17 adsorption and
283 inhibit the adsorption of phage HP3. A modified adsorption assay was utilized for this
284 experiment using ExPEC “coated” with mucin. Briefly, the bacteria were incubated in
285 different concentrations of mucin (0%-1.5%), pelleted, and washed to remove any
286 mucin that did not adhere to the bacterial surface (Figure 3Ci). Next, a standard
287 adsorption assay was conducted with phages ES17 and HP3. Interestingly, phage
288 ES17 showed no adsorption to ExPEC in 10 minutes in the absence of mucin; however,
289 if first incubated with 1.5% mucin, adsorption increased to 98% (Figure 3Cii). In
290 contrast, 98% of phage HP3 was adsorbed without mucin and the adsorption dropped
291 to 75% in its presence (Figure 3Ciii). Transmission electron microscopy (TEM) analysis
292 of these samples at 10 minutes demonstrated that only in the presence of mucin was
293 phage ES17 found bound to the bacterial surface (red arrows) (Fig 3Di-vi, 4 out of 11
294 images of ExPEC + mucin had visible evidence of ES17 compared to 0 out of 10 in the
295 absence of mucin). TEM imaging of phage HP3 adsorption showed the presence of
296 bound phage in images with and without mucin present (red arrows) (Figure S4Bi-ii). In
297 this case, 5/14 of the imaged fields showed phage HP3 bound with mucin-coated
298 ExPEC compared with 7/14 bound without mucin (Figure S4Biii). Finally, we adapted an
299 ELISA-like approach to determine if phage ES17 preferred binding to surfaces coated
300 with mucin, a hypothesis consistent with our data. Indeed, when mucin was bound to an
301 ELISA plate, phage ES17 bound to the mucin-surface at higher levels than phage HP3
302 (Figure 3E, $p = 0.041$ and $p = 0.002$). Taken together, using three different approaches,
303 these data obtained suggests that phage ES17 binds mucin, a property that may
304 enhance its ability to infect *E. coli* in mucin-rich environments.

305

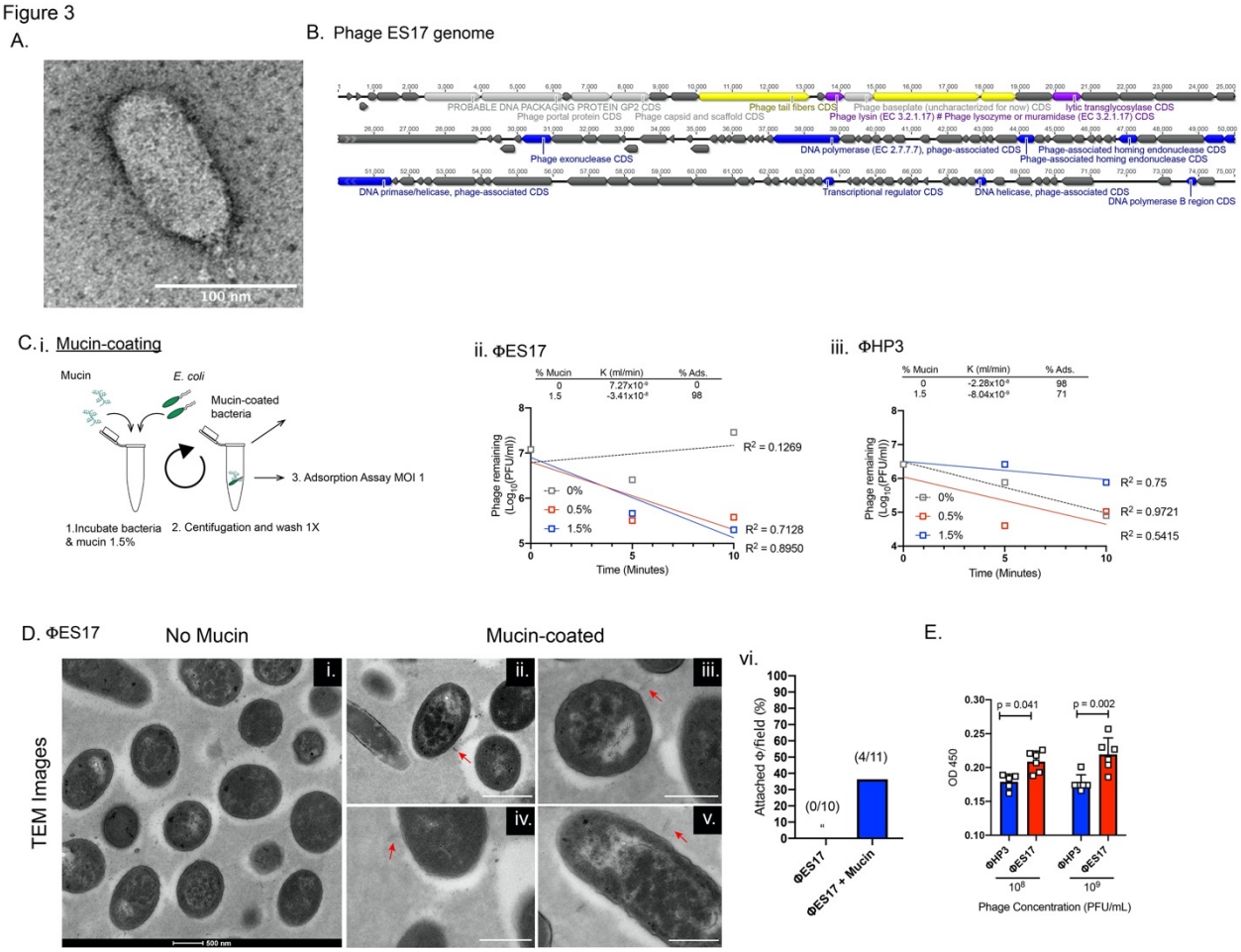

306

307 **Figure 3: Phage ES17 is a rare C3 type phage with avidity for mucin.** (A) TEM of ES17. (B)
308 Genome of ES17. (Ci) ExPEC was incubated in 0%, 0.5% and 1.5% mucin, centrifuged,
309 washed and phage added for an adsorption assay. (Cii) Phages ES17 and (Ciii) HP3
310 adsorption. Adsorption constant (K) and % adsorbed in 10 min indicated. Regression line
311 generated from mean values of phage remaining for time points indicated. (Di-v) TEM of phage
312 ES17 and ExPEC fixed after 10 min. adsorption. White bar is 500 nm. Red arrows indicate
313 phage (Dvi) Attached phages per field view. (E) Mucin-ELISA results for phages HP3 and ES17.
314 Squares indicate individual biological replicates from independent cultures. Exp. performed 1X
315 (C) and (D), 2X (E). N=6, " = none detected. Mean, ±SD shown.
316

317 **Phage ES17 may bind bacterial polysaccharides**

318

319 As indicated above, phage ES17 is a close relative of the kuravirus phiEco32 and

320 annotated as the same phage type. ES17's putative tail fiber protein (ES17-TFP)

321 showed high homology (64% identical) to a tail fiber protein in another lytic podophage,
322 the T7-like bacteriophage LM33_P1, which also targets ST131 strains (Dufour *et al.*,
323 2016). This homology is in the C-terminal receptor binding region (Figure S5Ai). The N-
324 terminal region is similar to vB_EcoP_WFI101126 (47% identical), a phage with C3 like
325 morphology similar to phage ES17 (Figure S5Aii)(Korf *et al.*, 2019). The T7-like phage
326 tail fibers have recently been characterized and shown to have knob-like tips, which we
327 also observed in the EM images of phage ES17 (Figure 3A) (Garcia-Doval and van
328 Raaij, 2012). T7-like phage tail fibers have been shown to possess endosialidases that
329 target surface sugars, such as capsule-forming polysaccharides (Garcia-Doval and van
330 Raaij, 2012). A BLAST analysis revealed that ES17-TFP contains a putative
331 pectinesterase (E value 7.45e-03, 369 bp) with high homology to phage lyases (Figure
332 4A). Modeling of the predicted structure of ES17-TFP indicated it may contain a pectin
333 lyase fold (Figure S5B, IPR011050). These lyases cleave bacterial polysaccharides and
334 are found in biofilm-degrading phages (Latka *et al.*, 2017). Additionally, this enzyme
335 was not found in phage HP3. Thus, we formed the hypothesis that ES17 might degrade
336 and infect biofilms.
337
338 ExPEC is a primary cause of catheter-associated UTI (CAUTI), often associated with
339 the formation of biofilms on the catheter (Russo and Johnson, 2003). For this study, we
340 used a clinical isolate (DS515) from a CAUTI patient, which forms significant biofilms *in*
341 *vitro* (data not shown). We tested the effect of various *E. coli* phages on DS515 biofilms
342 using a colorimetric assay with a metabolic substrate, MTT, to determine the sensitivity
343 of the biofilm bacteria to the phage (Figure 4B). As determined in Figure 4C, of the 10

344 *E. coli* phages assessed, which were shown to be lytic towards the clinical isolate, only
345 two phages significantly educed *E. coli* viability after establishment of the biofilm, and
346 only one of these three, ES17, reduced the biofilm by more than half. Since phage HP3
347 showed moderate levels of killing of *E. coli* in biofilms, we compared its ability to phage
348 ES17 over a 6-log titration range. Strikingly, as little as 10^3 PFU/ml of phage ES17
349 statistically reduced biofilm viability, which was greater than that achieved with 10^9
350 PFU/ml of phage HP3 (Figures 4Di-ii). In addition, phage ES17 showed a dose
351 dependent response at each concentration with the greatest effect seen at 10^9 PFU/ml
352 ($p < 0.0001$) (Figure 4Dii). Also, we found that phage ES17 formed large plaques with
353 halos on DS515 and related clinical isolates (picture above Figure 4Dii). This is in
354 contrast to phage HP3 which showed no halo formation (picture above Figure 4Di). This
355 halo formation is indicative of EPS (extracellular polymetric substance)-degrading
356 activity (Knecht, Veljkovic and Fieseler, 2020).
357
358 We reasoned ES17-TFP may be responsible for the cleavage of the EPS in the biofilm,
359 thereby allowing phage ES17 to gain access to *E. coli* in the biofilm. Thus, we cloned
360 the DNA encoding ES17-TFP into an expression vector and purified it from *E. coli*. A
361 highly induced band of the expected molecular weight of ES17-TFP (107 KDa) was
362 observed upon SDS-PAGE separation of the eluted fractions (Figure S5C). This band
363 was not observed in the vector only control elutions (data not shown). When ES17-TFP
364 was added to the biofilms, no change in bacterial viability was observed, nor did it
365 enhance ES17 killing of *E. coli* in biofilms when added separately (Figure 4E). Likewise,
366 when incubated in CM, or examined for its ability to degrade mucus using a gel-shift

assay in an anti-mucin Western blot, it did not enhance ES17 activity or degrade mucus (data not shown). Furthermore, phage ES17 by itself also did not demonstrate this activity. These data suggests that phage ES17's unique killing abilities are not dependent on degradation of polysaccharides (e.g. mucin or bacterial). This leaves open the question of how this tail fiber protein may enhance killing in carbohydrate-rich environments.

Figure 4

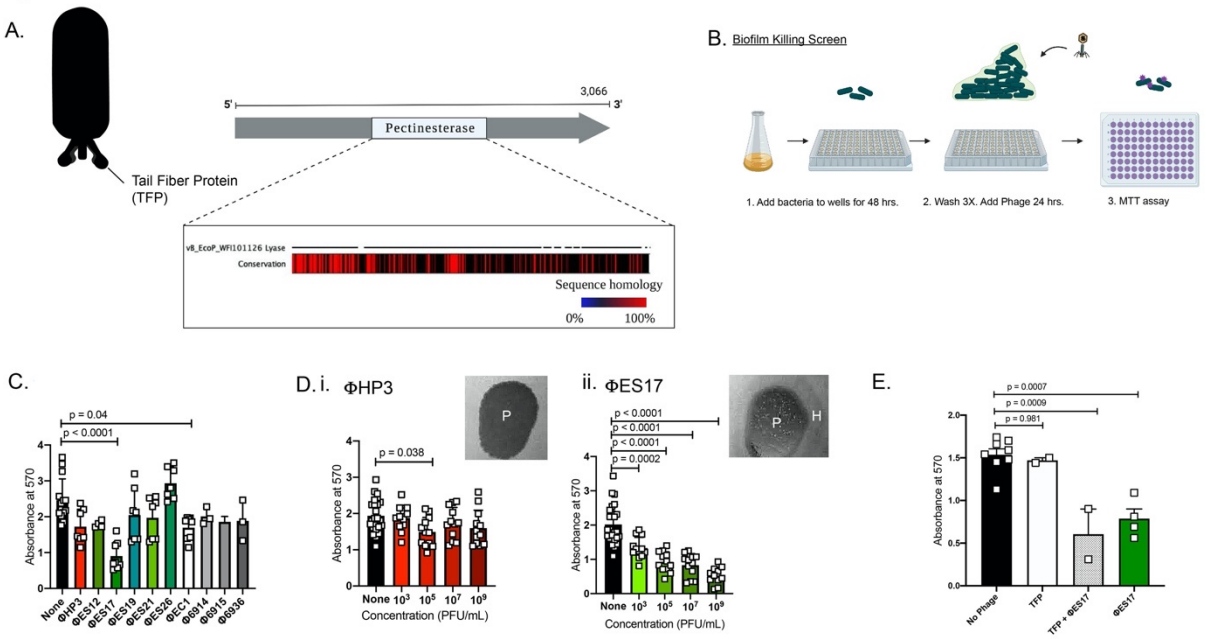

Figure 4: Phage ES17 may bind bacterial polysaccharides. (A) ES17 TFP domain compared to vB_EcoP_WFI101126 lyase. (B) DS515 was grown o/n in TSB and inoculated on a plate for 48-hr biofilm growth. A phage library was screened with MTT used to quantitate biofilm forming bacteria. (C) DS515 levels with phage library (N=3-8). (Di) DS515 levels with HP3 and (Dii) ES17 (N=12). Plaques "P" from phages on pictured with or without halo "H" (E) ExPEC levels with purified ES17-TFP in CM assay (N=2-8). Squares indicate individual biological replicates from independent cultures. Exp. performed 2X. Mean, ±SD shown. Figure created with BioRender.com.

Phage ES17 binds human heparan sulfated proteoglycans.

385 Phage ES17 harbors an enhanced ability relative to other *E. coli* phages to find its
386 bacterial host in environments in which carbohydrates are a prominent chemical
387 component (examples from above include cecal medium, mucin-rich broth, and
388 biofilms). A structural analysis of modeled ES17-TFP showed a high similarity to a
389 phage K5 lyase binding domain (E-value=4E-12). The predicted structure of ES17-TFP
390 (blue) and K5 lyase are pictured in Figure S6Ai (PDB:2X3H; red) with identical residues
391 colored yellow. Phage K5 binds K5 capsular polysaccharide and acts as a K5
392 polysaccharide lyase (Hanfling *et al.*, 1996). The K5 *E. coli* capsule is made of a
393 repeating disaccharide that is identical to the precursor of heparin and heparan sulfate
394 (HS), a linear polysaccharide, present in glycosaminoglycans (HSPGs, heparan sulfate
395 proteoglycans). (Figure S6Aii) These proteoglycans are found on mammalian cells and
396 in mucus (Monzon, Casalino-Matsuda and Forteza, 2006). Also, mucins with similar
397 structures to heparan sulfate/heparin (α-linked GlcNAC or N-Acetyl-D-glucosamine) are
398 present intestinally and found in PGM (Fujita *et al.*, 2011).
399
400 We reasoned that ES17's enhanced activity might be due to a novel ability to bind
401 mammalian polysaccharides found on glycoproteins. This would be a novel mechanism
402 by which a phage could localize to its host, thereby explaining its enhanced activity in a
403 mucin-rich environment and in EPS biofilms. To test this idea, we assessed the ability of
404 purified ES17-TFP to bind to a glycan array containing over ~ 860 unique glycan
405 structures from porcine gastric mucin (PGM), glycosaminoglycans (GAGs) and a variety
406 of synthetic and naturally sourced glycans generated by the Consortium for Functional
407 Glycomics (CFG) (see supplementary methods). No or very low relative fluorescent

408 units (RFU), a proxy for binding, was observed for a wide array of mammalian glycans,
409 including those purified from porcine gastric mucin (Figure S6Bi-ii). However,
410 surprisingly, there was an increase of several orders of magnitude in RFU (RFUs >
411 2000) observed for binding to the GAGs containing heparan sulfate (ID # 64-173), but
412 not the structurally similar GAGs hyaluronic acid #1-20 or chondroitin sulfate #21-63
413 (Figure S6Bii-iii). The finding that purified ES17-TFP binds human heparan sulfated
414 proteoglycans provides a possible mechanism to explain why phage ES17
415 demonstrates enhanced activity in intestinal environments.
416
417 **ES17 binds to the surface of human intestinal enteroids (HEIMs)**
418
419 Human intestinal enteroids (HIEs) are organotypic, higher-order cultures that have
420 become popular as surrogates to model the human intestine. They can be grown as 3-
421 dimensional structures complete with a lumen and crypt/villus axis or as 2-dimensional
422 monolayers that facilitate host-pathogen interactions (In *et al.*, 2016; Saxena *et al.*,
423 2016). These cultures are also useful because they express a variety of glycans found
424 in the human intestine, including mucins and proteoglycans (Saxena *et al.*, 2016).
425 Human intestinal enteroid monolayers (HIEMs) were derived from colonic stem cells
426 following differentiation for 5 days in high Wnt medium. Phage ES17 or HP3 were
427 added to confluent HIEMs for 1 hour, extensively washed, and visualized by
428 immunofluorescence microscopy using antibodies raised against each phage. Little to
429 no detectable phage HP3 was observed on the HIEMs intestinal epithelial cell (IEC)
430 surface, though antibodies generated robust signal and specificity towards the phage

431 when HP3 was fixed on slides alone (Figure 5A and S4C). Phage ES17 (green) bound
432 evenly to the IECs on the apical side, including areas where prominent Muc2 (red)
433 localization was observed, but also on areas where there was no muc staining (Figure
434 5Aii). In order to determine whether phage ES17 bound to the IECs of HIEMs via
435 heparan sulfate, we pre-treated the HIEMs with heparinase III to enzymatically remove
436 HSPGs and then assessed phage binding. Indeed, HIEMs treated with heparinase
437 significantly reduced the levels of bound ES17, both qualitatively and quantitatively
438 (Figures 5Bi-vii, $p < 0.0001$). Next, we tested whether this binding to the epithelial cell
439 surface also improved bacterial killing. Previous data had shown that ExPEC adheres
440 less to intestinal enteroids compared to the diarrhea-causing pathogen
441 Enteroaggregative *Escherichia coli* (EAEC) (data not shown). EAEC adheres to HIEMs
442 robustly in an aggregative, mesh-like pattern and similar to phage ES17 utilizes heparan
443 sulfate as a receptor to bind these human colonic cells (Rajan et al., 2020, paper *in*
444 *review*)(Poole, Rajan and Maresso, 2018; Rajan *et al.*, 2018). Thus, EAEC serves as an
445 ideal *E. coli* strain to test the hypothesis that phage targeting HSPGs can increase
446 killing. For this experiment we pre-coated HIEMs with phage ES17, washed, as detailed
447 above, then infected with EAEC strain 042. HIEMs were fixed and stained using a
448 Geimsa-Wright stain to visualize cells and bacteria, as previously described (Rajan *et*
449 *al.*, 2018). Infected HIEMs showed robust bacterial adhesion to cells with an
450 aggregative phenotype (Figure 5Cii, red arrows). Phage coated HEIMs, however,
451 showed significantly reduced EAEC on the surface of the organoid (Figure 5Ciii-iv, $^{**}p =$
452 0.007). Taken together, these data suggests phage ES17 may localize to both the
453 mucus layer and to the IEC surface by binding to HSPGs, which likely position the

454 phage to be in the exact location needed to find its bacterial target in the intestinal

455 microenvironment.

Figure 5

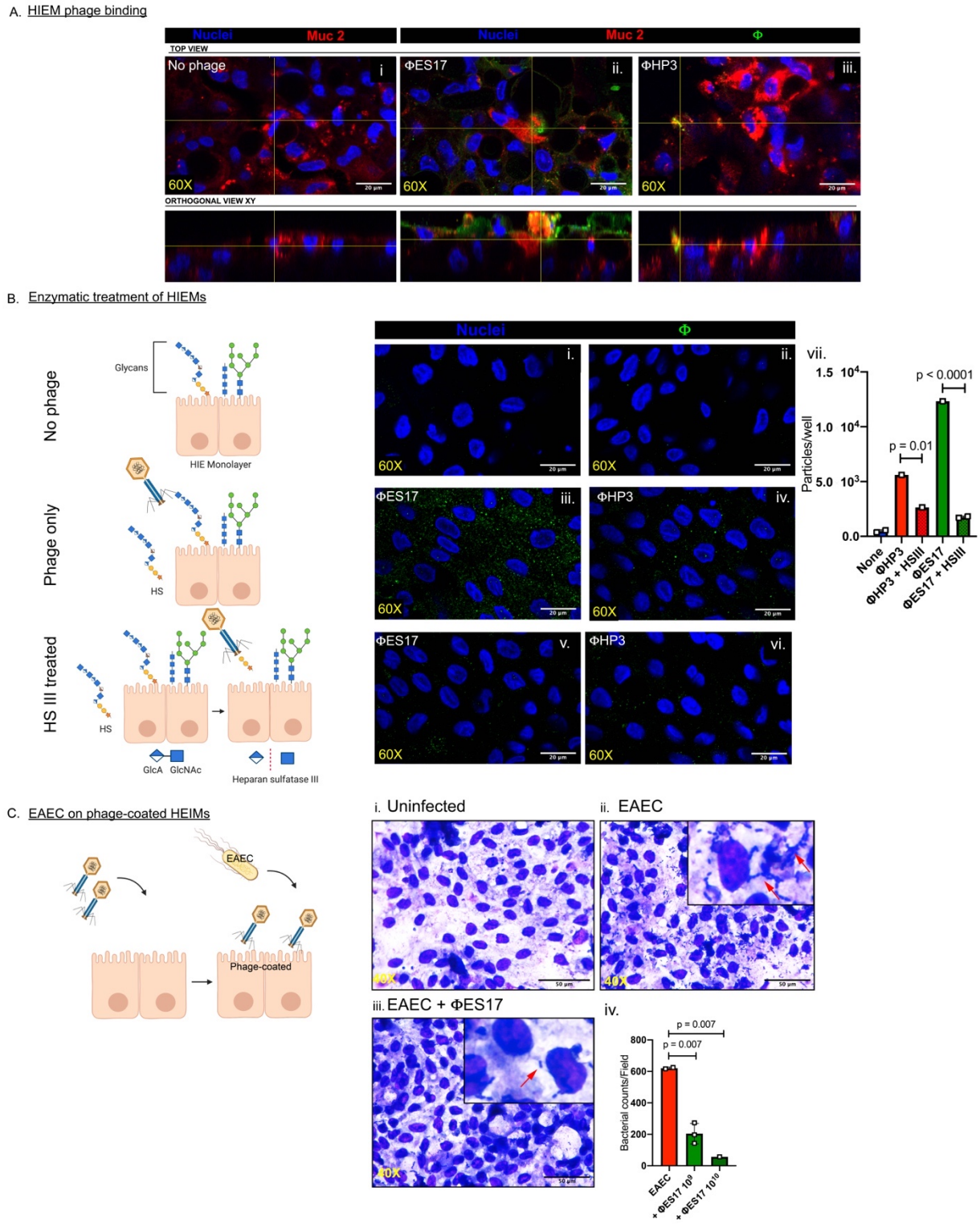

456

457
458
459 **Figure 5: ES17 binds to the surface of human intestinal enteroids (HIEMs)**. HIEMs were
460 incubated with phage for 1 hr, washed, then fixed and imaged for phage (Alexa Fluor 488,
461 Green), intestinal cells (DAPI, Blue), and muc2 (Alexa Fluor 594; Red). (Ai) No phage added.
462 (Aii) Phage ES17 or (Aiii) HP3 added. Monolayers pretreated with heparanase III then with
463 phage. (Bi, ii) No phage. (Biii) Phage ES17 and (Biv) phage HP3 added. (Bv) Hep III treated
464 HEIMs incubated with ES17 and (Bvi) HP3 (Bvii) Quantification of particles (phage) per well.
465 (N=1-2). Images at 60X. Scale bars at 20 μm. HIEMs (Ci) uninfected or (Cii) Infected with EAEC
466 042 (Ciii) or pretreated with phage ES17 prior to EAEC. Images at 60X. Scale bars at 50 μm.
467 (Civ) EAEC attached to HIEMs per field view. Mean, ±SD shown. Squares indicate individual
468 biological replicates from independent cultures. Exp. performed 1X. Figure created with
469 BioRender.com.
470

471 **Phage ES17 kills ExPEC in the mammalian intestine**

472

473 The finding that phage ES17 demonstrated enhanced lytic activity in the presence of
474 mucins, was the best of several screened phages in a mock luminal environment rich in
475 mucins, and binds the human organotypic culture IECs via HSPGs, which leads to
476 EAEC-killing on the bacterial surface, prompted an examination into whether this phage
477 could overcome the intestinal-induced inhibition of phage lytic activity towards colonized
478 ExPEC that was observed for phage HP3. We first tested if ES17 was effective in cecal
479 medium. Indeed, phage ES17 showed a 2.5-log improvement in ExPEC removal in this
480 environment compared to phage HP3 (Figure 6A, $p < 0.0001$). There was no effect on
481 the number of OTUs or the Shannon diversity index in this experiment, suggesting
482 phage ES17 was highly selective at removing only the target ExPEC strain (Figure 6Bi-
483 ii). We next tested the effect of phage ES17 on ExPEC in a murine intestine. Animals
484 were colonized with ExPEC as in Figure 1A and treated with either phage ES17 or HP3
485 (Figure 6C).The dose of phage was also increased from 10^9 PFU to 10^{10} to also
486 evaluate if giving more phage would improve HP3's ability to reduce ExPEC, especially

487 in more proximal segments as the phage slowly moves through the alimentary canal.
488 Examination of the small and large intestine on day 6 showed phage levels were high
489 across all groups (10^6-10^8 PFU/g intestinal tissue) (Figure 6D). Animals treated with
490 phage HP3 had no detectable CFU in small intestinal tissue (Figure 6E), but had
491 indistinguishable levels from that of the untreated control in the cecum. In contrast,
492 every animal treated with phage ES17, except one, had no detectable levels of ExPEC
493 in either the small or large intestine, suggesting that this lytic phage possess a unique
494 ability to target ExPEC in complex mucosal environments such as the large intestine.

Figure 6

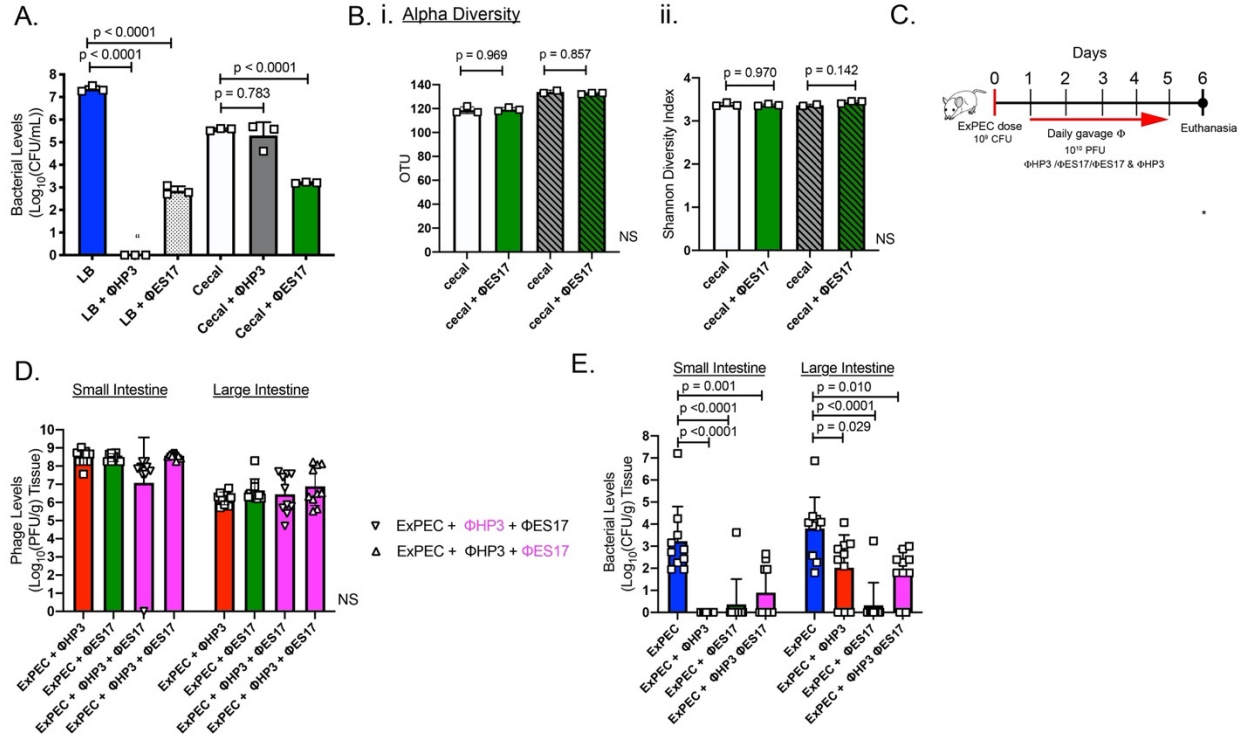

495

496

497 **Figure 6: ES17 kills in the mammalian intestine.** (A) ExPEC levels in CM assay with ES17
498 (N=3). 16S rRNA analysis of CM including (Bi) OTU and (Bii) Shannon diversity index. (C) Mice
499 were gavaged with ExPEC then treated with no phage or gavaged daily doses of phage HP3 at
500 10^{10} PFU, or ΦES17 at 10^{10} PFU or both phages ($2x10^{10}$ PFU total). (D) Intestinal (tissue) phage
501 levels (E) Intestinal (tissue) ExPEC levels. (N=10). Symbols (squares) indicate individual mice
502 or biological replicates derived from different cultures. Exp. performed 1X. NS not significant. " =
503 none detected. Mean, ±SD shown.

504

505 **Discussion**

506

507 A limitation of all antibiotics is their broad killing activity and no inherent features to
508 function well in complex human environments, including human blood, urine, or at
509 mucosal surfaces throughout the body. In particular, the gastrointestinal tract (GIT) is a
510 highly complex system made up of diverse organs and tissues and within that a
511 diversity of cell types. Some of the cells and factors found at the mucosal surface may
512 influence intestinal capacity including: intestinal epithelial cells, enteroendocrine cells,
513 stem cells, mucus-secreting goblet cells, antimicrobial peptides (AMPs – from Paneth
514 cells) and secretory immunoglobulin A (Mammarappallil and Elsinghorst, 2000;
515 Johansson, Larsson and Hansson, 2011; Sato *et al.*, 2011; Gribble and Reimann, 2016;
516 Pickard *et al.*, 2017). To add to this complexity, the GIT is colonized by a large number
517 of microbes—archaea, fungi, protists and bacteria that have co-evolved with the host,
518 termed the human gut microbiota (Pickard *et al.*, 2017; Heintz-Buschart and Wilmes,
519 2018). A bacteriophage would have to navigate through this complex ecosystem to find
520 and infect its host. Since there are estimated to be $>10^{10}$ PFU/g of phages already
521 present in the GIT, this suggests that phages can thrive in this environment (Hoyles *et*
522 *al.*, 2014; Shkoporov *et al.*, 2018). Here, we report a novel anti-bacterial targeting
523 strategy that seems to have evolved to position a lytic bacteriophage in the exact niche
524 as its bacterial host. Our results indicate that; (i) phage HP3 that is lytic towards *E. coli*
525 ST131 *in vitro* and is very effective at eliminating bacteremia in a murine model of
526 sepsis, is ineffective when tested for this same property in the murine intestinal tract; (ii)

527 that the inhibition is due to intestinal mucins; (iii) a medium designed to mimic the
528 luminal environment can be used to identify phage with enhanced lytic activity in such
529 an environment; (iv) a rare C3 type phage, isolated from human wastewater, overcomes
530 this inhibitory activity due to an enhanced ability of the phage to bind to heparan-
531 sulfated proteoglycans present in mucus or immobilized on the surface of intestinal
532 epithelial cells, which likely drives the positional targeting of the phage to the exact
533 ecological niche as the host bacterium. In addition, our data reveal that this treatment
534 when compared to antibiotic treatment, did not alter the intestinal diversity of the
535 microbiota. Taken together these data suggest a new mechanism of predation by a
536 phage, one which may be highly useful for the killing of bacteria in intestinal
537 environments and biofilms, both of which would be desirable properties of a targeted,
538 specific antibacterial.
539
540 Potential narrow or limited ecological range of bacteriophages has not been as explored
541 as much as their narrow host range capabilities. Using an experimental process of
542 elimination, we determined that mucin can greatly inhibit phage infection. Mucins are
543 composed of tandem repeats of serine and threonine that act as an attachment sites for
544 o-linked glycans (N-acetlygalactosamine, N-acetylglucosamine, fucose, galactose and
545 sialic acid) (McGuckin *et al.*, 2011; Wang and Hasnain, 2017). Gel-forming mucins,
546 which make up the mucus intestinal layer are large polymers (up to 40 MDa) of mucins
547 attached via disulfide linkages (McGuckin *et al.*, 2011). When we incubated phages with
548 porcine gastric mucin, composed of the gel-forming mucin MUC 5AC (Sturmer *et al.*,
549 2018), we saw reduced or no bacterial killing. However, when we added N-acetyl

550 cysteine (NAC), which is known to exert a mucolytic effect by reducing the disulfide
551 bonds that keep these mucin polymers together, bacterial killing was restored (Aruoma
552 *et al.*, 1989; Sadowska *et al.*, 2006). NAC is a drug has been tested and used in the
553 clinical setting to treat syndromes including cystic fibrosis (CF) and chronic obstructive
554 pulmonary disease (COPD). In both of these cases it loosens thick mucus in lungs, but
555 it can also serve as a treatment for acetaminophen overdose due to its antioxidant
556 action (Sadowska *et al.*, 2006; Saito, Zwingmann and Jaeschke, 2010; Bear, 2013).
557 Perhaps this drug could also be used as an adjuvant to phages to help treat patients
558 with bacterial infections in mucin-rich ecosystems such as the gut or the lungs of CF
559 patients. We tested oral NAC treatment in mice and found it to be more effective in
560 improving phage-mediated bacterial killing in the small intestine, but not in the large
561 intestine. NAC has been shown to be rapidly absorbed following oral dosing after only
562 60 minutes (Tsikas *et al.*, 1998). An oral dose of NAC has a short half-life of 2.5 hours
563 and 10% bioavailability in the gut (Tsikas *et al.*, 1998). It is likely that NAC did not exert
564 a mucolytic effect on the distal large intestine. Interestingly, we observed elevated
565 ExPEC levels in intestinal tissue with NAC treatment. It is possible that some pathogens
566 like ExPEC may thrive in environments with a reduced mucus layer.
567
568 Another possibility, distinct from adjuvating phage with NAC, would be to search for
569 phages that have evolved phenotypes that enhance their ability to encounter their
570 bacterial host in a specific ecosystem, such as the GIT. Phage ES17, originally isolated
571 from human sewage, is a member of the family *Podoviridae* and has a rare C3 type
572 elongated capsid morphology with paddle-like short tail fibers (Ackermann, 2001).

573 Previously, this phage was shown to be similar to PhiEco32, a rare Kuravirus which are
574 known for their prolate head (Gibson *et al.*, 2019). Phage ES17 showed a significant
575 killing effect in cecal medium (CM) and in a mouse model of intestinal colonization
576 compared to phage HP3. Phage ES17 bound mucin significantly better and coating
577 bacteria with mucin increased phage adsorption. There is precedence for this concept.
578 The bacteriophage adhering to mucus (BAM) model proposes that phages bind to
579 mucus via *hoc* proteins or Ig (immunoglobulin fold-like) domains present on the capsid
580 proteins of phages similar to T4 (Fraser *et al.*, 2006; Barr *et al.*, 2013, 2015). This
581 mechanism was suggested to explain how phages bind to the metazoan mucosal
582 surface and increase the probability of encountering a bacterial host, likely via a unique
583 type of controlled diffusion that increases spurious interactions with its bacterial target
584 (Barr *et al.*, 2013, 2015). These studies showed that T4 adsorption increased in the
585 presence of mucin from 65% to 80% absorbed phage within 10 minutes (Barr *et al.*,
586 2015). The adsorption changes in phage ES17 in the presence of mucin were all or
587 nothing from 0% to 98% within 10 minutes. This suggests that mucin may be a type of
588 "bridge receptor" for phage ES17 since this phage is ineffective at killing in the absence
589 of mucin, even at very high levels of phage. Such a model would make sense in the
590 context of *E. coli* embedded in a mucin matrix, perhaps breaking down mucin as a
591 source of carbon and thus binding it, thereby allowing the phage to adapt a capsular
592 polysaccharide binding mechanism to structurally related sugars that are prominent on
593 proteoglycans.
594

595 Bacteriophages have been shown to have a variety of carbohydrate-binding proteins
596 present on tail fibers in order to bind different sugars present on the bacterial cell
597 surface (Nobrega *et al.*, 2018). Some of the most diverse are capsular depolymerases,
598 which bind and break down capsular carbohydrates secreted by bacteria (Pires *et al.*,
599 2016). These capsular depolymerases are diverse because of the diversity of bacterial
600 capsule types. Capsule types have been shown to mimic some components of the
601 intestinal system, including sugars present in the mucus layer (Vimr and Lichtensteiger,
602 2002; Severi, Hood and Thomas, 2007). Bacteria can use these mechanisms to subvert
603 the immune system and to allow for the colonization of hosts (Vimr and Lichtensteiger,
604 2002; Kahya, Andrew and Yesilkaya, 2017). Phage ES17 was effective at killing
605 bacteria in biofilms and possessed a protein with putative capsular depolymerase
606 domains in a tail fiber protein. However, we could not detect any polysaccharide lyase
607 activity and instead detected strong and stable affinity for a human intestinal sugar, the
608 glycosaminoglycan sugar, heparan sulfate. This suggests a model whereby phage
609 ES17 adapted to “colonize” the mucosal environment by binding to mammalian sugars.
610 Heparan sulfate proteoglycans (HSPG) are expressed on the surface of many types of
611 cells and prominently on the surface of intestinal epithelial cells (Garcia *et al.*, 2016).
612 One of the more tantalizing discoveries here was that human enteroids derived from
613 colonic stem cells specifically bound phage ES17, but not other *E. coli* phages. HSPGs
614 consist of repeating units of sulfated polysaccharides—heparan sulfate (HS). HS is a
615 linear polysaccharide that begins as the precursor, heparan (disaccharide of α1,4-linked
616 N-acetylglucosamine (GlcNAc) and β1,4-linked glucuronic acid (GlcUA)) (Sugahara and
617 Kitagawa, 2002; Murphy *et al.*, 2004). Subsequent modifications due to sulfation and

618 epimerization leads to the mature form polysaccharide HS (Murphy *et al.*, 2004).
619 Bacteriophage K5 utilizes a tail spike lyase (*KflA*) to bind and degrade K5 capsule
620 present on *E. coli* strains (Hanfling *et al.*, 1996). Because the K5 capsule (heparoson;
621 β1,4-linked GlcUA and α1,4-linked GlcNAc) polysaccharide has been shown to be
622 structurally identical to heparan sulfate precursor, heparan, this enzyme can also act a
623 heparinase (Hanfling *et al.*, 1996; Roberts, 1996; Murphy *et al.*, 2004; O'Leary, Xu and
624 Liu, 2013). K5 heparan lyase cleaves the linkage of N-acetyl glucosamine and
625 glucuronic acid, but is inhibited by sulfated regions (Murphy *et al.*, 2004; O'Leary, Xu
626 and Liu, 2013). Further homology searches showed that the carbohydrate binding
627 domain found in ES17-TFP is structurally homologous to the binding domain present in
628 the tail spike in phage K5. Considering that heparanase III cleaves at the same regions
629 where K5 lyase would bind and degrades suggests ES17-TFP is utilizing the same
630 receptor. Indeed, the addition of heparanse III, from the soil bacteria *Flavobacterium*
631 *heparinum*, which specifically cleaves unmodified (unsulfated) NAc domains (GlcNAc-
632 GlcUA) and NA/NS domains (GlcNS (N-Sulfo-D-Glucosamine) and GlcNAc) of HS,
633 leads to abrogated phage ES17 binding to cells, meaning ES17 was highly specific for
634 this type of glycan (Murphy *et al.*, 2004; Park *et al.*, 2017). Structurally similar mucins to
635 heparan sulfate (Class III type, α-linked GlcNAc) suggest that this protein may also
636 target these intestinal mucins (Ota *et al.*, 1998; Fujita *et al.*, 2011). This interaction is
637 driven by phage ES17's tail fiber protein, which is not related to the *hoc* proteins or
638 contain an Ig-like fold as predicted from the BAM model. Thus, it would seem that
639 phage ES17 uses a novel mechanism to localize not only a mucin-rich surface, but also
640 directly to the mammalian epithelial surface (Figure 7). It is worth speculating that not

641 only would this be a way to intercept *E. coli* that would also colonize this surface, but it
642 could also be exploited therapeutically as a prophylactic “epithelium protecting” coating
643 that prevents the pathobiont from invading the mucosa. Several pathogens, including
644 bacteria and human pathogenic viruses have been shown to bind to HS and use them
645 as receptors (Alvarez-Dominguez *et al.*, 1997; Fleckenstein, Holland and Hasty, 2002;
646 Cagno *et al.*, 2019). It is tempting to speculate that this property might have been also
647 acquired by phage, as suggested here.

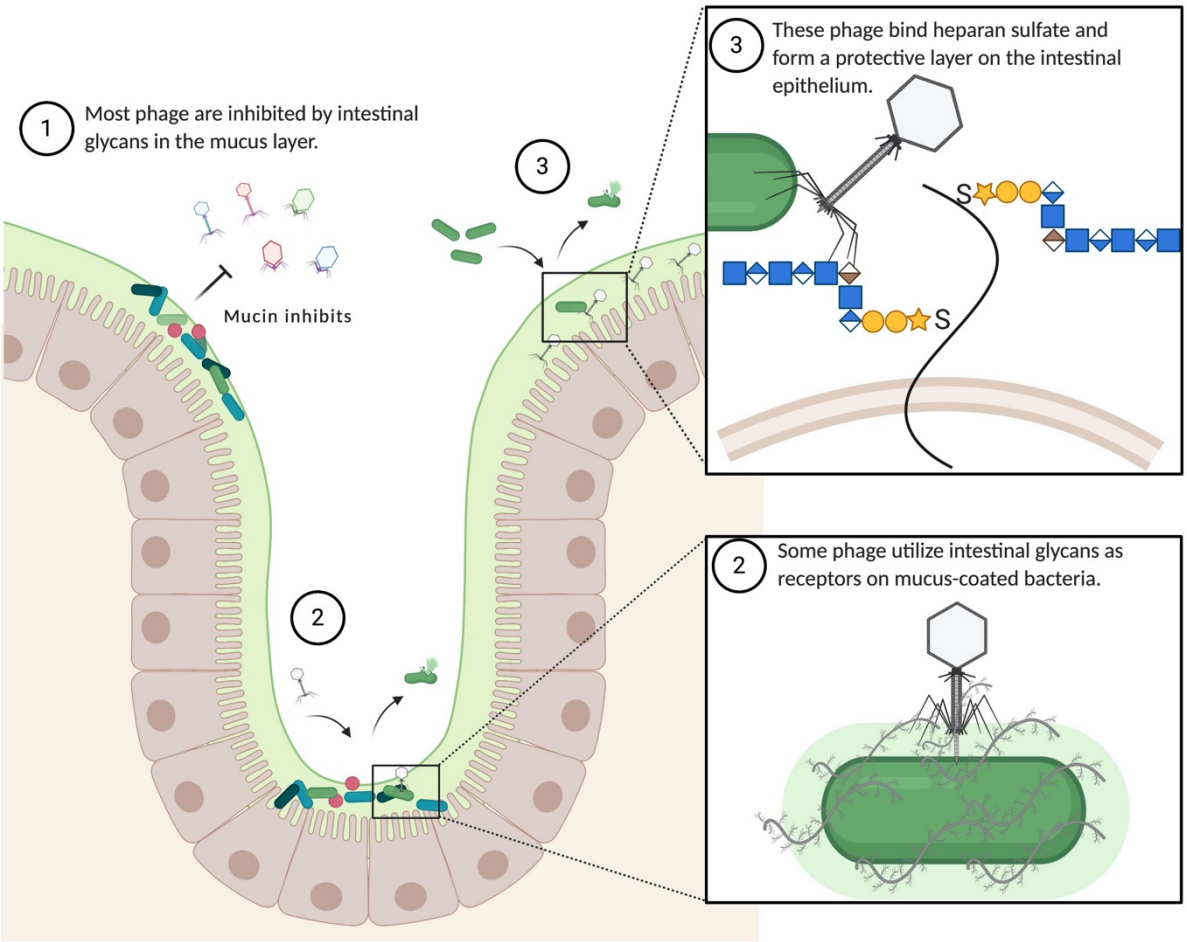

648

649 **Figure 7:** Model showing (1) mucins from the intestinal mucus layer inhibit phage infection, (2)
650 phage ES17 can bind to mucin and utilize other intestinal glycans as a receptor to infect and kill
651 mucus-coated bacteria, and (3) phages like ES17 can be utilized to coat the intestinal
652 epithelium by binding heparan sulfate glycans to protect from invasive pathogen infection.
653 Figure created with BioRender.com.
654

655

656

657 **Materials and Methods**

658

659 Bacterial strains and phages

660

661 ExPEC ST131 isolate JJ1901 was used in all ExPEC infections, except Figure S1Aiii
662 (JJ2528). Both isolates were previously obtained from Dr. Jim Johnson (University of
663 Minnesota)(Green *et al.*, 2017b). Commensal *E. coli* ECN (Figure S1iv) was isolated
664 from a human fecal sample. Deidentified strain DS515 is a clinical isolate obtained from
665 the clinical microbiology laboratory at the Houston Veterans Administration Hospital.
666 Prior to infections all strains were grown overnight at 37°C from a single colony streaked
667 on an LB agar plate. The intestinal pathogen EAEC 042 (serotype 44:H18), was
668 originally isolated from a child in Peru, and extensively characterized (Nataro *et al.*,
669 1985).

670

671 Phages HP3, ES12, ES17, ES19, ES21 and ES26 have been previously described and
672 characterized (Green *et al.*, 2017a; Gibson *et al.*, 2019). Phage 6914, 6915 and 6939
673 were recently isolated from sewage. All phages described in Table 1 were isolated by
674 single plaque isolation from environmental sources as described previously (Green *et*
675 *al.*, 2017b; Gibson *et al.*, 2019).

676

677 Murine infections

678

679 Mixed ages (6-10 months) and sexes of BALB/c (Jackson laboratories, Bar Harbor, ME)
680 mice were used in mouse models of infection. Mice were kept in SPF environment at
681 Baylor College of Medicine CCM (Center for Comparative Medicine) Taub facility. All
682 methods performed on mice were approved in accordance with relevant guidelines and
683 regulations from "The Guide and Care and Use of Laboratory Animals" (National
684 Institute of Health) and approved by Baylor College of Medicine's Institutional Animal
685 Care and Use Committee (protocol AN-6372). For infections mice were kept in a
686 biohazard facility with sterile food and water. The mice were individually housed during
687 colonization experiments and bedding replaced with autoclaved techboard liners for
688 daily fecal collection. For colonization experiments, sample size was determined based
689 on previous colonization experiments in mice (Green *et al.*, 2017a). Mice received a 10^9
690 CFU dose of ExPEC strain JJ1901 via oral gavage. Rodent health was monitored daily
691 for indication of pain or disease. Bacterial colonization (fecal and intestinal) was
692 determined after homogenization and selective plating for the chloramphenicol resistant
693 strain JJ1901 on LB agar plates containing chloramphenicol and colony counting.
694 Purified phage in 3% (m/v) $NaHCO_3$ was administered either via gavage or in water 5%
695 (m/v) sucrose added *ad libitum*. All groups received sucrose and $NaHCO_3$ in water for
696 consistency. The antibiotic ampicillin (1g/500 ml) was administered in water. Phage
697 colonization was quantified after dilution of homogenates and serial plating on a double
698 agar overlay assay.

699

700 *Ex vivo* cecal model

701

702 A modified cecal assay was used for experiments (Theriot *et al.*, 2014). Briefly, cecal
703 contents from just euthanized mice were pooled and homogenized in sterile 0.09%
704 NaCl solution at a 1:5 dilution (mg:mls). The homogenate was centrifuged to remove
705 large particulates (2000 G for 30 sec.). The supernatant fluid was used for 4.5 hr phage
706 killing assays at an MOI of 10 at 37°C, shaking (255 RPM), as previously described (Ma
707 *et al.*, 2018). All cecal and mucin experiments were performed using independent
708 bacterial cultures grown up from different colonies streaked on a plate. This was
709 considered a biological replicate. For FS CM, cecal supernatant was centrifuged (6000
710 G for 5 min.) and filtered through a 0.22 μm syringe filter. For HT CM, the supernatant
711 was heated at 100°F for 20 min in a hot water bath, then cooled to RT for infections.
712 Insoluble CM and soluble CM (supernatant) were isolated post high-speed
713 centrifugation (9000 G for 5 min) of CM. The insoluble pellet was resuspended in sterile
714 0.09% NaCl solution for infections (IN CM). For the mucin assays, porcine gastric mucin
715 type II (PGM; Sigma-Aldrich) was used at various concentrations diluted in phosphate
716 buffered saline (PBS). The mucolytic drug N-acetyl cysteine (NAC, Sigma-Aldrich, 5
717 mg/ml) was diluted in PBS for de-mucolytic assays.

718

719 Phage Sequencing and Annotation

720

721 The annotation figure was generated from previous data (Gibson *et al.*, 2019) using
722 Geneious Prime 2019.2.3 and adjusted in Inkscape.

723

724 Mucin-coating Adsorption and Imaging

725

726 For the adsorption curves, assays were performed at an MOI of 1 using mid-log phase
727 cultures independently grown from different colonies on a plate (this was considered a
728 biological replicate) and samples taken every 5 min for 10 min. Prior to adsorption, PGM
729 (0%, 0.5% and 1.5% m/v) was added to the bacterial cultures for 10 min. RT, shaking
730 (255 RPM). The cultures were centrifuged (6000 G for 5 min) and gently washed with
731 PBS. The adsorption rate constants (K) were determined from the natural log of the
732 slope of the adsorption curve versus the bacterial concentration. Some cultures were
733 fixed in glutaraldehyde solution after 10 min adsorption for TEM imaging. TEM imaging
734 was performed at the Texas Children's Hospital Center for Digestive Diseases. After
735 fixation the samples were dehydrated in ethanol and followed by evaporation of ethanol
736 and coating with gold for observation during TEM.

737

738 Mucin Binding ELISA Assay

739

740 Clear-walled Immulon 2 HB 96-well microtiter plate (Immunochemistry Technologies
741 #227) were used for the ELISA assays. PGM (200 μl of 1mg/ml) was added to a
742 microtiter plate and incubated at 4°C overnight. The next day the mucin was removed
743 and wells were washed twice with PBS. The phage was added to wells for 1 hr then
744 washed three times in PBST (PBS with 0.1% Tween-20). The wells were blocked with
745 BSA then incubated with antibodies for the phage overnight at 4°C. Following washing
746 steps, a HRP (horse radish peroxidase) conjugated antibody was added for 1 hr. To

747 assess phage binding, TMB solution was added until the wells turned light blue and
748 then a stop solution (2M H_2SO_4) was added. The absorbance was read at 450 nm. Each
749 well was considered a biological replicate for this experiment.
750
751 Biofilm Screening
752
753 Biofilm experiments were recently described but with some modifications (Mapes *et al.*,
754 2016). *E. coli* DS515 cultures were independently grown from different colonies on an
755 agar plate in tryptic soy broth (TSB) were diluted to an OD of 0.1 and seeded to
756 inoculate a 96 well plate for the biofilm formation assay. Each well was considered a
757 biological replicate. The plates were incubated statically at 37°C for 48 hrs. Following
758 incubation, planktonic cells were removed, and the wells were washed three times in
759 PBS. Phages diluted in TSB to 10^9 PFU/ml were added and incubated for 24 hrs at
760 37°C statically. The wells were washed three times in PBS then an MTT assay was
761 performed to determine the metabolic activity of the phage resistant biofilm-forming
762 bacteria. Protein quantification was determined using a Bradford assay (Biorad) using
763 BSA as a standard. Purified ES17-TFP was added at a concentration of 0.17 mg/ml to
764 biofilms with added phage.
765
766 HIEM Infection and Imaging
767
768 Human enteroid monolayers (HIEMs) were differentiated for 5 days (>90% confluent) as
769 described (Poole, Rajan and Maresso, 2018). For experiments each well containing

770 HIEMs was considered a biological replicate. HIEMs were incubated with phage at 10^8
771 PFU/ml in culture differentiation media for 1 hour at 37°C in the presence of 5% CO_2 in
772 a humidified incubator, then washed in PBS. The HIEMs were fixed in Clark's solution
773 for 10 min to preserve the mucus layer. The HIEMs were permeabilized and blocked
774 with 5% BSA in 0.1% Triton X-100 in PBS for 30 min at RT. Mucus was detected using
775 antibodies to MUC2 (1:200) (Abcam) and nuclei stained with 4′, 6′-diamidino-2-
776 phenylindole (DAPI) (300 nM) for 5 min at RT. Antibodies against phages HP3 and
777 ES17 were generated from whole virus (phage) injection into rabbits performed by
778 Pacific Immunology. A 13 week antibody production protocol consisted of 4
779 immunizations and anti-sera collection.
780
781 To selectively removed HSPG from GAG chains, enteroid cultures were pretreated with
782 heparinase III (Sigma, 2U/ml) for 2 hours, as described (Jiao *et al.*, 2007), followed by the
783 addition of phage. Images were captured using a Zeiss LSM 510 confocal microscope.
784 Represented images were adjusted equally for brightness and contrast using FIJI
785 software version 2.0.0. The images were adjusted equally for brightness and contrast.
786 Particle analysis was used to determine particles per well. The Cell counter program in
787 FIJI was used to quantitate bacteria (EAEC) per field of view.
788
789 EAEC infection and staining
790
791 For infection of HIEMs, the EAEC strain 042 was grown overnight and then sub-cultured
792 (1:100) for 2 hrs at 37°C. One microliter of the log-phase bacterial culture was added to

793 100 microliters of the cell culture media and added to chambered slides either with
794 phage-coated HIEMs (as described above) or untreated. Cultures were incubated for
795 3.5 hrs at 37°C in the presence of 5% CO_2 in a humidified incubator. Following growth,
796 bacteria were removed, by gently washing the cells in PBS then the remaining cells
797 were fixed (Hema 3 fixative) and stained using a Geimsa-Wright stain (Fisher scientific).
798 The infection and staining technique have been previously described (Rajan *et al.*,
799 2018).
800
801 Statistics
802
803 Statistical analysis was performed using PRISM 8 software. Microbiome 16S data was
804 analyzed using ATIMA (Agile Toolkit for Incisive Microbial Analyses) as described in
805 supplemental methods. For figures with log transformed data and groups >2
806 significance was determined using a one-way ANOVA analysis (Figures 1, 2, 3, 4, 5 and
807 6) or two way ANOVA when necessary (Figure 3E). For multiple comparison analysis,
808 the secondary test, Tukey, was used. For non-transformed data a normality test
809 (Shapiro-Wilk) was performed to determine normality before a one-way ANOVA
810 analysis was performed. Significance was determined to be a p value less than or equal
811 to 0.05. Unless otherwise stated all graphs show the mean and standard deviation.
812
813 **Acknowledgements**
814

This work is supported in part by grant from US Veterans Affairs (VA I01-RX002595), Roderick D. MacDonald Research Fund at Baylor St. Luke's Medical Center, the Mike Hogg Foundation, and Seed Funds from Baylor College of Medicine Seed Fund

We would like to thank Dr. Melinda Engevik for general expertise and protocol help related to mucin work. We would also like to thank Hannah Johnson from the Integrated Microscopy Core at Baylor College of Medicine for technical assistance related to imaging.

Author Contributions

S.G., C.L., X.Y., W.S., A.R., H.C. and X.S. performed experiments and analyzed data. J.C. performed bioinformatics studies. R.R., B.T., and H.K., contributed to design of studies and edited the manuscript. S.G. designed studies and wrote the manuscript. A.M. contributed to design and overall major goals of the study and edited the manuscript.

References

Ackermann, H. W. (2001). Frequency of morphological phage descriptions in the year 2000. Arch. Virol. *5*, 843–857.

838 Alvarez-Dominguez, C. *et al.* (1997). Host cell heparan sulfate proteoglycans mediate
839 attachment and entry of Listeria monocytogenes, and the listerial surface protein ActA is
840 involved in heparan sulfate receptor recognition. Infect. Immun. *1*, 78–88.
841
842 Antão, E.M., Wieler, L. H. and Ewers, C. (2009). Adhesive threads of extraintestinal
843 pathogenic *Escherichia coli*. Gut. Pathog. *1*, 22.
844
845 Aruoma, O. I. *et al.* (1989). The antioxidant action of N-acetylcysteine: its reaction with
846 hydrogen peroxide, hydroxyl radical, superoxide, and hypochlorous acid. Free Radic.
847 Biol. Med. *6*, 593–597.
848
849 Banerjee, R. and Johnson, J. R. (2014). A new clone sweeps clean: The enigmatic
850 emergence of *Escherichia coli* sequence type 131. Antimicrob. Agents CH. *9*, 4997-
851 5004.
852
853 Barr, J. J. *et al.* (2013). Bacteriophage adhering to mucus provide a non-host-derived
854 immunity. Proc. Natl. Acad. Sci*. 26*, 10771–10776.
855
856 Barr, J. J. *et al.* (2015). Subdiffusive motion of bacteriophage in mucosal surfaces
857 increases the frequency of bacterial encounters, Proc. Natl. Acad. Sci. *44*, 13675–
858 13680.
859
860 Bear, C. E. (2013). 50 years ago in the Journal of Pediatrics: the effect of N-

861 acetylcysteine on the viscosity of tracheobronchial secretions in cystic fibrosis of the
862 pancreas, J. Pediatr. *1*, 85.
863
864 Brum, J. R. *et al.* (2016). Illuminating structural proteins in viral “dark matter” with
865 metaproteomics. Proc. Natl. Acad. Sci. *9*, 2436-2441.
866
867 Cagno, V. *et al.* (2019). Heparan Sulfate Proteoglycans and Viral Attachment: True
868 Receptors or Adaptation Bias? Viruses. *7*. 596.
869
870 Carlstedt, I. *et al.* (1993). Characterization of two different glycosylated domains from
871 the insoluble mucin complex of rat small intestine. J. Biol. *25*, 18771-18781.
872
873 Chang, D. E. *et al.* (2004). Carbon nutrition of *Escherichia coli* in the mouse intestine.
874 Proc. Natl. Acad. Sci. *19*, 7427-7432.
875
876 Colpan, A. *et al.* (2013). *Escherichia coli* sequence type 131 (ST131) subclone h30 as
877 an emergent multidrug-resistant pathogen among US Veterans. Clin. Infect. Dis. *9*,
878 1256-1265.
879
880 Dedrick, R. M. *et al.* (2019). Engineered bacteriophages for treatment of a patient with a
881 disseminated drug-resistant Mycobacterium abscessus. Nat. Med. *5*, 730-733.
882
883 Dufour, N. *et al.* (2016). Bacteriophage LM33_P1, a fast-acting weapon against the

884 pandemic ST131-O25b: H4 *Escherichia coli* clonal complex. J. Antimicrob. *11*, 3072-
885 3080.
886
887 Fleckenstein, J. M., Holland, J. T. and Hasty, D. L. (2002). Interaction of an Outer
888 Membrane Protein of Enterotoxigenic *Escherichia coli* with Cell Surface Heparan
889 Sulfate Proteoglycans. Infect. Immun. *3*, 1530–1537.
890
891 Fraser, J. S. *et al.* (2006). Ig-like domains on bacteriophages: a tale of promiscuity and
892 deceit. J. Mol. Biol. *2*, 496–507.
893
894 Fujita, M. *et al.* (2011). Glycoside hydrolase family 89 α-N-acetylglucosaminidase from
895 clostridium perfringens specifically acts on GlcNAcα1,4Galβ1R at the non-reducing
896 terminus of O-glycans in fastric mucin. J .Biol. Chem. *8*, 6479-6489.
897
898 Garcia-Doval, C. and van Raaij, M. J. (2012). Structure of the receptor-binding carboxy-
899 terminal domain of bacteriophage T7 tail fibers. Proc. Natl. Acad. Sci .U S A. *24*, 9390–
900 9395.
901
902 Garcia, B. *et al.* (2016). Surface Proteoglycans as Mediators in Bacterial Pathogens
903 Infections. Front. Microbiol. *7*, 220.
904
905 Gibson, S. B. *et al.* (2019). Constructing and Characterizing Bacteriophage Libraries for
906 Phage Therapy of Human Infections. Front. Microbiol. *10,* 2537.

907

908 Green, S. I. *et al.* (2017a). Bacteriophages from ExPEC Reservoirs Kill Pandemic
909 Multidrug-Resistant Strains of Clonal Group ST131 in Animal Models of Bacteremia. Sci
910 Rep. *7*, 46151.

911

912 Gribble, F. M. and Reimann, F. (2016). Enteroendocrine Cells: Chemosensors in the
913 Intestinal Epithelium. Annu. Rev. Physiol. *78*, 277–299.

914

915 Grose, J. H. and Casjens, S. R. (2014). Understanding the enormous diversity of
916 bacteriophages: The tailed phages that infect the bacterial family Enterobacteriaceae,
917 Virology. *468*, 421–443.

918

919 Hanfling, P. *et al.* (1996). Analysis of the enzymatic cleavage (beta elimination) of the
920 capsular K5 polysaccharide of *Escherichia coli* by the K5-specific coliphage:
921 reexamination. J. Bacteriol. *15*, 4747–4750.

922

923 Heintz-Buschart, A. and Wilmes, P. (2018). Human Gut Microbiome: Function Matters.
924 Trends Microbiol. *7*, 563–574.

925

926 Hoyles, L. *et al.* (2014). Characterization of virus-like particles associated with the
927 human faecal and caecal microbiota. Res. Microbiol. *10*, 803–812.

928

929 Huang, S. H. *et al.* (2001). A novel genetic island of meningitic *Escherichia coli* K1

930 containing the ibeA invasion gene (GimA): Functional annotation and carbon-source-
931 regulated invasion of human brain microvascular endothelial cells. Funct. Integr.
932 Genomic. *5*, 312-322.
933
934 In, J. G. *et al.* (2016). Human mini-guts: New insights into intestinal physiology and
935 host-pathogen interactions. Nat. Rev. Gastroenterol. Hepatol. *11*, 633–642.
936
937 Jault, P. *et al.* (2019). Efficacy and tolerability of a cocktail of bacteriophages to treat
938 burn wounds infected by *Pseudomonas aeruginosa* (PhagoBurn): a randomised,
939 controlled, double-blind phase 1/2 trial. Lancet Infect. Dis. *1*, 35-45.
940
941 Jiao, X. *et al.* (2007). Heparan sulfate proteoglycans (HSPGs) modulate BMP2
942 osteogenic bioactivity in C2C12 cells. J. Biol. Chem. *2*, 1080–1086.
943
944 Johansson, M. E. V. and Hansson, G. C. (2016). Immunological aspects of intestinal
945 mucus and mucins. Nat. Rev. Immunol. *10*, 639–649.
946
947 Johansson, M. E. V., Larsson, J. M. H. and Hansson, G. C. (2011). The two mucus
948 layers of colon are organized by the MUC2 mucin, whereas the outer layer is a
949 legislator of host-microbial interactions. Proc. Natl. Acad. Sci. *108*, 4659–4665.
950
951 Johnson, J. R. *et al.* (2013). Abrupt emergence of a single dominant multidrug-resistant
952 strain of *Escherichia coli*. J. Infect. *6*, 919-928.

953

954 Johnson JR, R. T. (2002). Extraintestinal pathogenic *Escherichia coli:* "The other bad *E*
955 *coli*". J. Lab. Clin. Med*. 3,* 155-162*.*

956

957 Kahya, H. F., Andrew, P. W. and Yesilkaya, H. (2017). Deacetylation of sialic acid by
958 esterases potentiates pneumococcal neuraminidase activity for mucin utilization,
959 colonization and virulence. PLOS Pathog. *3*, e1006263

960

961 Knecht, L. E., Veljkovic, M. and Fieseler, L. (2020). Diversity and Function of Phage
962 Encoded Depolymerases. Front. Microbiol. *10*, 29449.

963

964 Korf, I. H. E. *et al.* (2019). Still Something to Discover: Novel Insights into *Escherichia*
965 *coli* Phage Diversity and Taxonomy. Viruses. *5*, 454.

966

967 Latka, A. *et al.* (2017). Bacteriophage-encoded virion-associated enzymes to overcome
968 the carbohydrate barriers during the infection process. Appl. Microbiol. *8*, 3103-3119.

969

970 Loc-Carrillo, C. and Abedon, S. T. (2011). Pros and cons of phage therapy.
971 Bacteriophage. *2*, 111-114.

972

973 Ma, L. *et al.* (2018). Metals Enhance the Killing of Bacteria by Bacteriophage in Human
974 Blood. Sci. Rep.*1,* 2326*.*

975

976 Mammarappallil, J. G. and Elsinghorst, E. A. (2000). Epithelial Cell Adherence Mediated
977 by the Enterotoxigenic *Escherichia coli* Tia Protein, *12*, 6595–6601.
978
979 Mapes, A. C. *et al.* (2016). Development of expanded host range phage active on
980 biofilms of multi-drug resistant *Pseudomonas aeruginosa*. Bacteriophage. 1, e1096995.
981
982
983 De Martel, C. *et al.* (2012). Global burden of cancers attributable to infections in 2008: A
984 review and synthetic analysis. Lancet Oncol. *6*, 607-615.
985
986 Maruvada, P. *et al.* (2017). The Human Microbiome and Obesity: Moving beyond
987 Associations. Cell Host Microbe. *5*, 589-599.
988
989 Mathers, A. J., Peirano, G. and Pitout, J. D. (2015). *Escherichia coli* ST131: The
990 quintessential example of an international multiresistant high-risk clone. Adv. Appl.
991 Microbiol. *90*, 109–154.
992
993 McGuckin, M. A. *et al.* (2011). Mucin dynamics and enteric pathogens. Nat. Rev
994 Microbiol. *4*, 265–278.
995
996 Mitsuoka, T., Hayakawa, K. and Kimura, N. (1975). The fecal flora of man, Zentralbl
997 Bakteriol. Orig. A. *4*, 499–511.
998

999 Monzon, M. E., Casalino-Matsuda, S. and Forteza, R. M. (2006). Identification of
1000 glycosaminoglycans in human airway secretions. Am. J. Resp. Cell. Mol. *2*, 135–141.
1001
1002 Moye, Z. D., Woolston, J. and Sulakvelidze, A. (2018). Bacteriophage applications for
1003 food production and processing. Viruses. *2*, 135.
1004
1005 Murphy, K. J. *et al.* (2004). A new model for the domain structure of heparan sulfate
1006 based on the novel specificity of K5 lyase. J. Biol. Chem. *26*, 27239–27245.
1007
1008 Nataro, J. P. *et al.* (1985). Detection of an adherence factor of enteropathogenic
1009 *Escherichia coli* with a dna probe. J. Infect. *3*, 560-565.
1010
1011 Nataro, J. P. (2005) *Colonization of Mucosal Surfaces*. Edited by W. N. J. Nataro,
1012 James P. Cohen S. Paul, Mobley L.T. Harry. ASM. doi: 10.1128/9781555817619.
1013
1014 Nicolas-Chanoine, M. H., Bertrand, X. and Madec, J. Y. (2014). *Escherichia coli* st131,
1015 an intriguing clonal group. Clin. Microbiol. Rev. *3*, 543-574.
1016
1017 Nobrega, F. L. *et al.* (2018). Targeting mechanisms of tailed bacteriophages. Nat. Rev.
1018 Microbiol. *12*, 760–773.
1019
1020 O'Leary, T. R., Xu, Y. and Liu, J. (2013). Investigation of the substrate specificity of K5
1021 lyase A from K5A bacteriophage. J. Glycobiol.*1*, 132–141.

1022

1023 O'Neill, J. (2016). Antimicrobial Resistance : Tackling a crisis for the health and wealth
1024 of nations, Review on Antimicrobial Resistance.

1025

1026 Ota, H. *et al.* (1998). New monoclonal antibodies against gastric gland mucous cell-type
1027 mucins: A comparative immunohistochemical study. Histochem Cell Biol. 2, 113-119.

1028

1029 Park, H. *et al.* (2017). Heparan sulfate proteoglycans (HSPGs) and chondroitin sulfate
1030 proteoglycans (CSPGs) function as endocytic receptors for an internalizing anti-nucleic
1031 acid antibody. Sci .Rep.*1*, 14373.

1032

1033 Pickard, J. M. *et al.* (2017). Gut microbiota: Role in pathogen colonization, immune
1034 responses, and inflammatory disease. Immunol. Rev. *1*, 70–89.

1035

1036 Pires, D. P. *et al.* (2016). Bacteriophage-encoded depolymerases: their diversity and
1037 biotechnological applications. Appl. Microbiol .Biotechnol. *5*, 2141–2151.

1038

1039 Pitout, J. D. D. (2012). Extraintestinal pathogenic *Escherichia coli:* A combination of
1040 virulence with antibiotic resistance. Front. Microbiol. *3*, 9.

1041

1042 Poole, N. M. *et al.* (2017). Role for FimH in extraintestinal pathogenic *Escherichia coli*
1043 invasion and translocation through the intestinal epithelium. Infect. Immun. *11*. e00581-
1044 17.

1045

1046

1047 Poole, N. M., Rajan, A. and Maresso, A. W. (2018). Human Intestinal Enteroids for the
1048 Study of Bacterial Adherence, Invasion, and Translocation. Curr. Protoc. Microbiol. *1*,
1049 55.

1050

1051 Poolman, J. T. and Wacker, M. (2016). Extraintestinal pathogenic *Escherichia coli*, a
1052 common human pathogen: challenges for vaccine development and progress in the
1053 field. J. Infect. *1*, 6–13.

1054

1055 Price, L. B. *et al.* (2013). The epidemic of extended-spectrum-β-lactamase-producing
1056 *Escherichia coli* ST131 is driven by a single highly pathogenic subclone, H30-Rx. mBio.
1057 6, e00377-13.

1058

1059 Rajan, A. *et al.* (2018). Novel segment- and host-specific patterns of enteroaggregative
1060 *Escherichia coli* adherence to human intestinal enteroids. mBio. 1, e02419-17.

1061

1062

1063 Ren, H. *et al.* (2019). Genome sequence analysis of Vibrio parahaemolyticus lytic
1064 phage Vp_R1 with a C3 morphotype. Arch. Virol. *11*, 2865–2871.

1065

1066 Roberts, I. S. (1996). The biochemistry and genetics of capsular polysaccharide
1067 production in bacteria. Annu. Rev. Microbiol. *50*, 285–315.

1068

1069 Russo, T. A. and Johnson, J. R. (2003). Medical and economic impact of extraintestinal
1070 infections due to Escherichia coli: focus on an increasingly important endemic problem,
1071 Microbes. Infect. *5*, 449–456.

1072

1073 Sadowska, A. M. *et al.* (2006). Role of N-acetylcysteine in the management of COPD,
1074 Int. J. Chron. Obstruct. Pulmon. Dis. *4*, 425–434.

1075

1076 Saito, C., Zwingmann, C. and Jaeschke, H. (2010). Novel mechanisms of protection
1077 against acetaminophen hepatotoxicity in mice by glutathione and N-acetylcysteine.
1078 Hepatology.*1*, 246–254.

1079

1080 Sampson, T. R. and Mazmanian, S. K. (2015). Control of brain development, function,
1081 and behavior by the microbiome. Cell Host Microbe. *5*, 565–576.

1082

1083 Sansonetti, P. J. (2004). War and peace at mucosal surfaces. Nat. Rev. Immunol. *12*,
1084 953–964.

1085

1086 Sato, T. *et al.* (2011). Paneth cells constitute the niche for Lgr5 stem cells in intestinal
1087 crypts. Nature. *7330*, 415–418.

1088

1089 Sausset, R. *et al.* (2020). New insights into intestinal phages. Mucosal Immunol. 2, 205–
1090 215.

1091

1092 Savalia, D. *et al.* (2008). Genomic and Proteomic Analysis of phiEco32, a Novel
1093 *Escherichia coli* Bacteriophage. J. Mol. Biol. *3*, 774–789.

1094

1095 Saxena, K. *et al.* (2016). Human Intestinal Enteroids: a New Model To Study Human
1096 Rotavirus Infection, Host Restriction, and Pathophysiology. J. Virol.*1*, 43–56.

1097

1098 Schooley, R. T. *et al.* (2017). Development and use of personalized bacteriophage-
1099 based therapeutic cocktails to treat a patient with a disseminated resistant
1100 Acinetobacter baumannii infection. Antimicrob. Agents Chemother. 10, e00954-17.

1101

1102 Severi, E., Hood, D. W. and Thomas, G. H. (2007). Sialic acid utilization by bacterial
1103 pathogens. Microbiology. *9*, 2817–2822.

1104

1105 Shkoporov, A. N. *et al.* (2018). Reproducible protocols for metagenomic analysis of
1106 human faecal phageomes. Microbiome. *1*, 68.

1107

1108 Shkoporov, A. N. and Hill, C. (2019). Bacteriophages of the Human Gut: The “Known
1109 Unknown” of the Microbiome. Cell Host Microbe. *2*, 195–209.

1110

1111 Sturmer, R. *et al.* (2018). Commercial Porcine Gastric Mucin Preparations, also Used as
1112 Artificial Saliva, are a Rich Source for the Lectin TFF2: In Vitro Binding Studies.
1113 Chembiochem, *24*, 2598–2608.

1114

1115 Sugahara, K. and Kitagawa, H. (2002). Heparin and heparan sulfate biosynthesis,
1116 IUBMB Life. *4*, 163–175.

1117

1118 Tang, W. H. W., Li, D. Y. and Hazen, S. L. (2019). Dietary metabolism, the gut
1119 microbiome, and heart failure. Nat. Rev. Cardiol. *3*, 137–154.

1120

1121 Terwilliger, A. L. *et al.* (2020). Tailored Antibacterials and Innovative Laboratories for
1122 Phage (Φ) Research: Personalized Infectious Disease Medicine for the Most Vulnerable
1123 At-Risk Patients. PHAGE. 2, 66-74.

1124

1125 Theriot, C. M. *et al.* (2014). Antibiotic-induced shifts in the mouse gut microbiome and
1126 metabolome increase susceptibility to Clostridium difficile infection. Nat. Commun. *5*,
1127 3114.

1128

1129 Tsikas, D. *et al.* (1998). Analysis of cysteine and N-acetylcysteine in human plasma by
1130 high-performance liquid chromatography at the basal state and after oral administration
1131 of N-acetylcysteine. J. Chromatogr. B. Biomed. Sci. Appl. *1–2*, 55–60.

1132

1133 Vatanen, T. *et al.* (2018). The human gut microbiome in early-onset type 1 diabetes
1134 from the TEDDY study. Nature. *7728*, 589–594.

1135

1136 Vimr, E. and Lichtensteiger, C. (2002). To sialylate, or not to sialylate: that is the

1137 question. Trends Microbiol. *6*, 254–257.

1138

1139 Wang, R. and Hasnain, S. (2017). Analyzing the Properties of Murine Intestinal Mucins

1140 by Electrophoresis and Histology. BIO-PROTOCOL. doi: 10.21769/bioprotoc.2394.

1141

1142 Youle, M., Haynes, M. and Rohwer, F. (2012). Scratching the surface of biology's dark

1143 matter. Viruses. doi: 10.1007/978-94-007-4899-6_4.

1144

1145 **Tables**

Table 1. Properties of E. coli phages used in mucin screen.

Phages	**ΦES12**	**ΦES17**	**ΦES19**	**ΦJ2W**	**ΦJ3M**	**ΦJ1M**	**ΦJ1S**	**ΦUlt1**	**ΦShp1**	**ΦM1M**	**ΦM1S**	**ΦT1S**
Source	Human	Human	Human	Human	Human	Human	Human	Human	Sheep	Rabbit	Rabbit	Pigs
Source location	Sewage	Sewage	Sewage	Sewage	Sewage	Sewage	Sewage	Sewage	Animal facility	Animal facility	Animal facility	Animal facility
Isolation strain	JJ2050	JJ2547	DS104	JJ2528	JJ2528	JJ2528	JJ2528	JJ1901	JJ1901	JJ1901	JJ1901	JJ1901
Plaque size (mm)	0.5	0.5 – 1.0	0.5	0.5	0.5	0.5	0.5	0.5 – 1.0	0.5	0.5	0.5	0.5
Plaque morphology	Clear	Clear, halo	Clear, halo	Clear, halo	Clear	Clear	Clear	Clear	Clear	Clear	Clear	Clear
ST131 lysed (%)[a.]	9/13 (69)	9/13 (69)	11/13 (85)	-	-	-	-	12/13 (92)	12/13 (92)	11/13 (85)	12/13 (92)	10/13 (77)
Accession #	MN508614	MN508616	MN508617	-	-	-	-	-	-	-	-	-

[a.] ExPEC ST131 library of isolates described previously (Gibson et al., 2019).

1146

1147

1148

1149

1150

1151

1152

1153

1154

Supplemental Figures, Methods and References

Figure S1

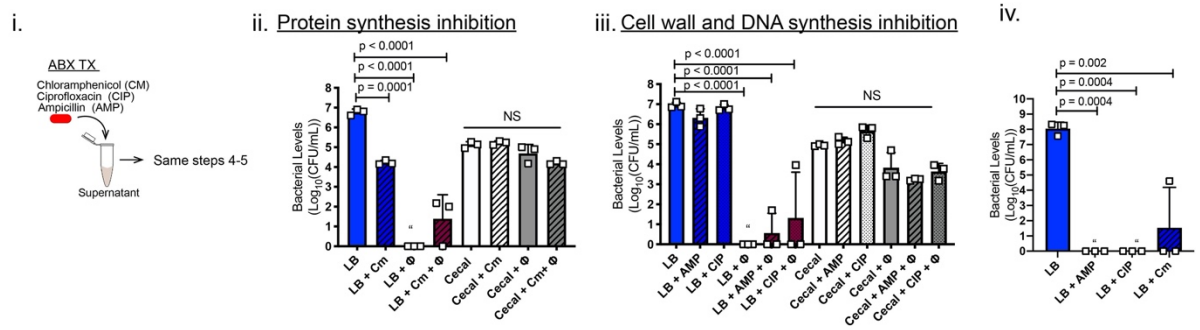

Figure S1 (i) ExPEC levels in CM assay incubated with antibiotics (ii) chloramphenicol (Cm) ciprofloxacin (CIP) or (iii) ampicillin (AMP). (iv) Commensal bacterial levels incubated in antibiotics indicated. (N=3-5). Exp. performed 1X. Squares indicate individual biological replicates from independent cultures. NS not significant.“ = none detected. Mean, ±SD shown.

Figure S2

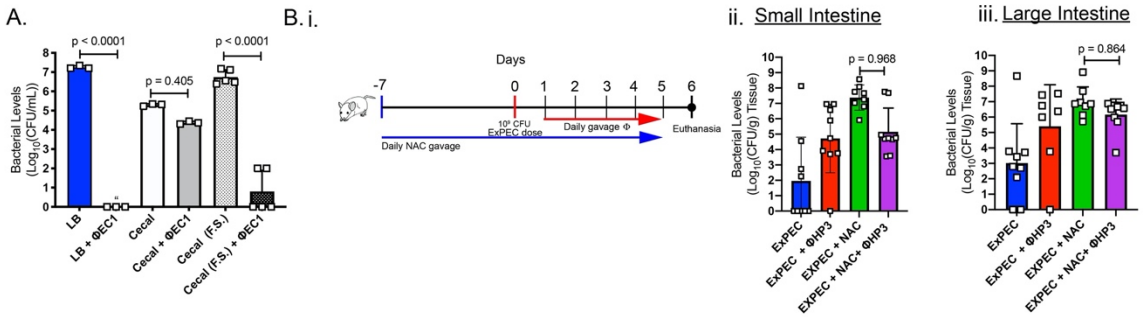

Figure S2 (A) ExPEC levels in CM (FS) with phage EC.1. (N=3) (Bi) Mice were gavaged daily with N-acetyl cysteine for 2 weeks. ExPEC was gavaged on day 0 following protocol from Figure 1A. (Bii) Small intestinal ExPEC levels. (Biii) Large intestinal ExPEC levels. (N=9). Exp. performed 1X. Squares indicate individual biological replicates from independent cultures or individual mice. NS not significant.“ = none detected. Mean, ±SD shown.

Figure S3

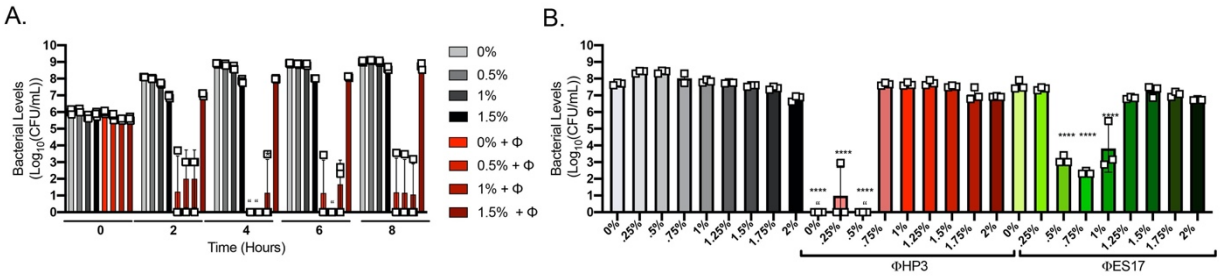

1171 **Figure S3** (A) ExPEC levels from 0 to 8 hours in LB plus mucin concentrations indicated and +/-
1172 phage HP3. (B) ExPEC levels with phages HP3 or ES17 (MOI of 10) in LB plus mucin
1173 concentrations indicated. (N=3). ****p < 0.0001. " = none detected. Exp. performed 1X. Squares
1174 indicate individual biological replicates from independent cultures. Mean, ±SD shown.
1175

Figure S4

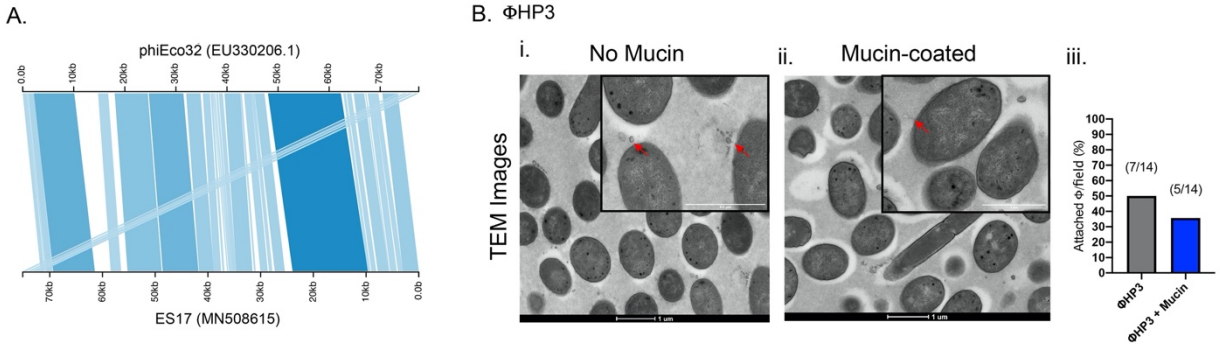

1176

1177

1178 **Figure S4** (A) Graphical representation of BLAST analysis of phage ES17 (bottom axis;
1179 MN508615) and phage phiECo32 (top axis; EU330206.1) using Kablammo web-based software
1180 (Wintersinger and Wasmuth, 2015). Trapezoids drawn between the axis indicate individual
1181 BLAST alignments between the two sequences. The stronger alignments are shaded darker.
1182 (Bi-ii) TEM images of phage HP3 on ExPEC fixed 10 min post-incubation. White bar scale is 1
1183 μm. Red arrows indicate phage. (Bii) Quantification of attached phages per field view. Mean,
1184 ±SD shown.
1185

Figure S5

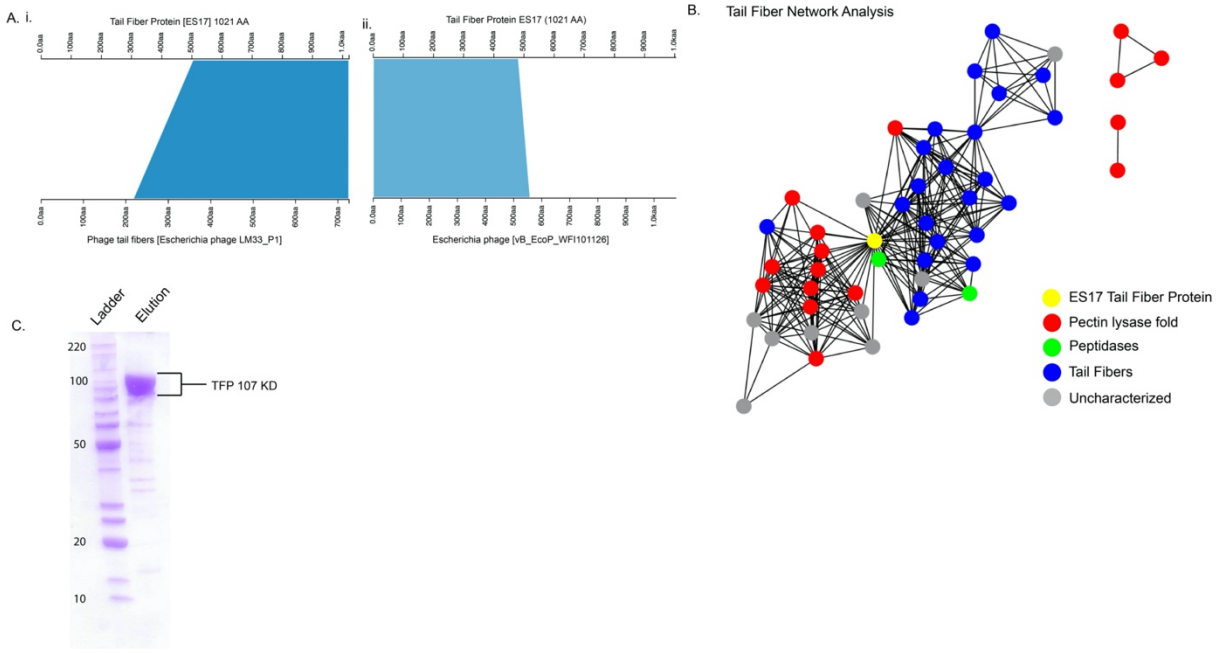

1186

1187 **Figure S5** (Ai) BLAST analysis of ES17-TFP (top axis) and phage LM33_P1 tail fiber (bottom
1188 axis, ref|YP_009324518.1|)) and (Aii) *E. coli* phage vB_EcoP_WFI101126 tail fiber (bottom axis,
1189 gb|QBQ76440.1|) (B) Network pictured. An E-value of 1E-1 was used as a cut off for node
1190 inclusion. Each node represents a single protein. Edges connect nodes with a BLAST E-value
1191 of less than 1E-10. The yellow node is the ES17-TFP, red nodes are proteins that belong to the
1192 pectin lysase fold/virulence factor family (IP011050), green nodes are proteins that are
1193 predicted peptidases; blue nodes are phage tail fibers; and gray nodes are uncharacterized
1194 proteins. (C) Protein SDS-PAGE gel showing purified ES-TFP pooled elutions and protein
1195 ladder.

Figure S6

A. TFP predicted structure comparison to K5 lyase

i.

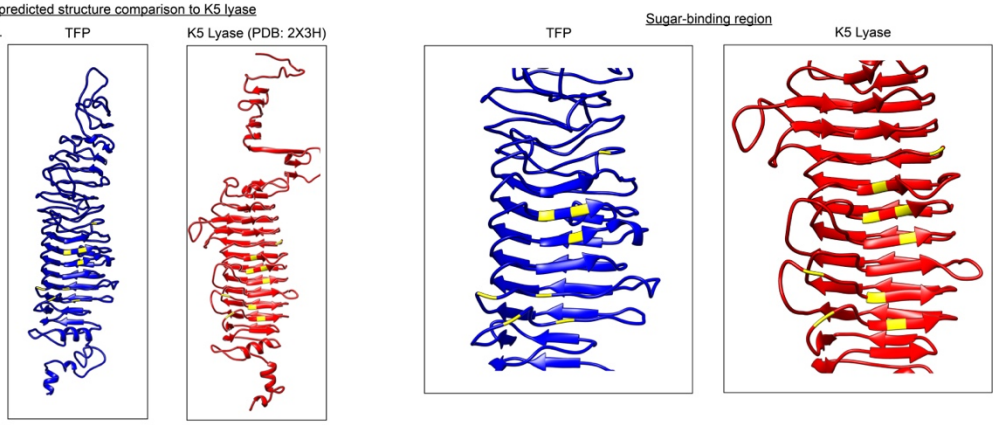

ii.

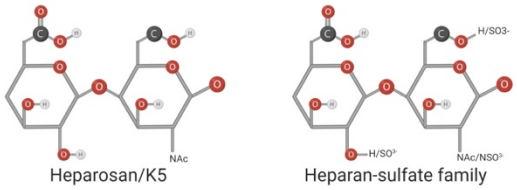

B. Glycan Microarray

i. PGM Array (Porcine Gastric Mucin)

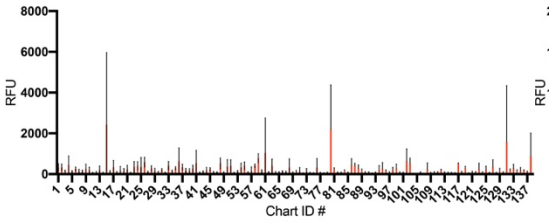

ii. CF Array

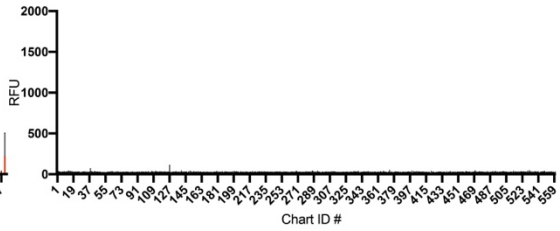

iii. Glycosaminoglycans (GAGs)

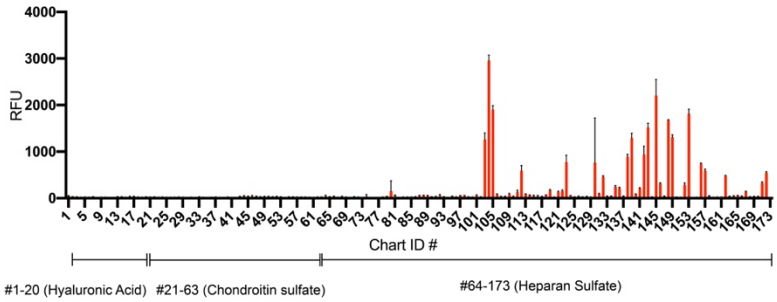

C. HP3 antibody specificity

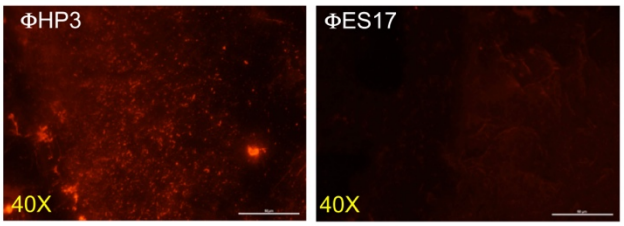

1196

1197 **Figure S6** (Ai) Structures show the predicted structure of tail fiber (blue), the structure of K5
1198 lyase (PDB:2X3H; red). Identical residues between K5 lyase and ES17 tail fiber protein are
1199 yellow. (Aii) Structures of heparosan or K5 capsule and heparan-sulfate derivative. (B) Glycan
1200 microarray analysis in relative fluorescent units (RFUs) using purified ES17-TFP as the GBP
1201 (glycan binding protein) and glycans derived from purified (Bi) porcine gastric mucin, (Bii) other
1202 mammalian glycans (CF array, see methods) and (Biii) glycosaminoglycans. N=3. Experiment
1203 was performed 3X. (C) Immunofluorescent staining of ES17 and HP3 phages fixed on a slide
1204 using antibodies generated against HP3 and secondary fluorescently conjugated (Alexa Fluor
1205 594; Red).
1206

1207 **Supplemental Methods**

1208

1209 Antibiotic treated CM

1210

1211 For antibiotic treated cecal medium, CM was incubated with chloramphenicol (10
1212 ug/mL, EMD Millipore) or ampicillin sodium salt (100 ug/mL) or ciprofloxacin (10 ug/mL)
1213 throughout the 4.5 hour infection using ExPEC JJ1901 (Figure S1ii) or JJ2528 (Figure
1214 S1iii) or commensal *E. coli* ECN (Figure S1iv).

1215

1216 NAC Mouse Model

1217

1218 Mice (BALB/c) were housed individually and gavaged daily with NAC (N-acetyl cysteine)
1219 at a concentration of 40 mg/mouse/day throughout the experiment as indicated (14
1220 days). This was a tolerable concentration and shown to be effective in the mouse small
1221 intestine (De Lisle, Roach and Jansson, 2007). Mice were infected as described in the
1222 primary methods, then euthanized on day 6 and plated to determine bacterial
1223 concentration in the intestinal contents.

1224

1225 Genome Comparison

1226 Genome comparison was performed using a BLAST analysis of phage ES17

1227 (MN508615) and phiECO32 (EU330206.1) and visualized using Kablammo software

1228 (Wintersinger and Wasmuth, 2015).

1229

1230 ES17-TFP Construct Generation

1231

1232 The construct used to purify tail fiber protein (TFP) was prepared by Genewiz (South

1233 Plainfield, NJ) using established protocols. The construct sequence for TFP was

1234 synthesized from the phage ES17 sequence (MN508615.1) nucleotides 58,576-61,641,

1235 ttaacgcagggcacgtctactattagcgaagcgcatagcctctgcctgagtagtgaactccgctacgaagtaatcagcga

1236 ggcgtaggactactccgcctgtaccggctgtacttaggcgcaggttcactgaaccggaagcactagcctgagctacacca

1237 aaggtactcacccactggcccccccttagtaaatacttcacctacattgatatctccaccgatgcggaagtttgtaggggttcc

1238 ctgtaccagttcagtgctaatgccccatacataccagttaccggaagttatctgaaatgcagcaccagtaagctcatactca

1239 gcagcaccagggatttcgaagtacatgcagctctgagataactggccttgtggctgcaaactcccagtgctgcttgccgta

1240 ccactaaattcagcagtacctccatcgaagggtttaactaccagcttattaccaggtacacgatagatgtatccttccggca

1241 ggtatccacgcatactcatattaggtgtccagctttgcccaatcttgcctgtctgagccgctacagaacgtaccattacatcttt

1242 gccggagctaccattcaggtacaattgatcagccacaaaactgctgttggcatctacagagatatccatgtggccatctga

1243 attatctactcggcagccataagtaacaaggttggagttctgaagctctacgttattaaggtatgtgtactctgcaaagaagat

1244 actggtatcaataagtttaaggacacgaggcttctgagatacaccatctacattaatagctggagtagtagcgatagcttcc

1245 atccatacattggatacaccacatggggcagtagggcagtcaccatccttgttcttgaggtaaataccaccaccgccaga

1246 ggcttccataatactatctttaatccaccagccgcctacaccacctccgaatgtaccaggcgcttctcctgttgtagcgttcaa

1247 gtaaacacagtaagtgctaataccatcaaagtgcatgttctgaagggtgtcagagcctaagtgcatctcagaagcagact

1248 gtgcccagtaaccccagtcacaaccttgcacgccaatgcctttccatgtattacctatattcccggaaggtttctgaatggcct

1249 tgttaatgttatggatgtatacgtcactaaagttgtgacgaccagcatattggtcggtcgggtcaaaactaatacctacagcc

1250 ccggttgtcccagaaccatctatagcaaaaccaccactatggcggaattgccaatgaggcgtagatgccttaacctgaat

1251 agtgtctgtaaagtttgacggagctttcagtaccgtggctccaccaacaccctttaactgtgtactaccaatagtaatcgcttc

1252 actgtattcaccgggggaaacaattaagtcgtttttttggtaacgatgcatttaccgcagcttgtaaggtagggaaatctcctga

1253 atgcttaatgtcgttgttacggacaagcaaacttctctcaccactgccaatgtttttagccccatctttactggaaagactctca

1254 acagaattaccattttcaaaggtaataagggatgcaccttcacctgcattactactttcagccttgccagcaaatctgcttca

1255 cttgtatgcaactgtctcaaagcaaccgcgtcattatcatctacagcatcaggaattactggagattgtgtgaaagtaacctt

1256 gttggtcatcgaggtgatatcagagttatcaccactcttagctgcaactagagctagtcgagcattctctgatgaagtagctcc

1257 tgtaccacctttggtaataggtacaattgattcagtggaaaccaaacctaaaccaagtttagtacgtgcagcacttgcagta

1258 gttgcccctgtgccaccctgagagatagtcacagggcgagcggaagacagctcttctcgtactgtaaatactcgggaacc

1259 aactcctccagtccagcttacagagaaaactgagtagtagttattattgtttgtccctggcaccactcgtacctcacctcctcct

1260 gtaactacgccaatgacttcaagatataacccataattggcaggataatttatctcagcaggggcatttgtaatattcgacatt

1261 aatactgaatagttacctccattgacaaaattaaatgtttgccagtccatagccttcactttggttaaggtagggctaccaatcc

1262 catgctcagcgagtccaatatttgtaatagctgcacttgtgtcggttatttcggataggttattagttacactaaaagctcccact

1263 tgagcagctgtgtagtctccagtagcaggaactacagcacccttacgtccattgaatgtggagacagaatcaaaaaccac

1264 tgaacctgtttgttcagcgccgccattgattgaaacagatcgaacagatggaatcaagttggcaatatctgacatgtcagct

1265 cggtataaaccaccatcatctttatctacatagaaaccatagtcatcaacaacaggggtaccaacaggaacgcttccaat

1266 atcaccgattgttccgtcagtaccatcacgccccggtttaccttctggaataccaaaagcaaagacacctgttgcattatcat

1267 aagaccccgtagctaggcttcccggaggaagaagcgttgtttgaactgtcatgttagagataatgtcaagttgtgctagaac

1268 gttttgagttgcctcttttgaaagctcagttgctgcattggtgttgtcaattgcagttcctgtggattgaatcaaacctaagagcac

1269 ttgttcttgtgactcaaagtcactcttgagttgtttaatgtcttcttccagtagatgaccttgagcatacagacgttctacttcagcc

1270 aaaatctcctctactgaggagtatttagtttgggacaacaatgcccaatatttagagtctgctgcatattcagctgctgatttata
1271 agcaccaatagttccctcagtagctccaaattgtcctacattgttaacattcttaggtgcttggttgttataaacgatcat.
1272
1273 This sequence was ligated onto pET-21b (+) (ampicillin) vector using restriction
1274 enzymes 5' *BamHI* and 3' *XhoI* by recombination and delivered as a mini-scale DNA
1275 sample.
1276
1277 Protein Purification
1278
1279 BL21 (DE3) cells were used for expression of His_6-TFP under the control of a T7
1280 promoter expression. Cells were induced with Isopropyl ß-D-1-thiogalactopyranoside
1281 (IPTG) 1mM for 2 hrs at 37°C. Then the culture was pelleted at 7000 RPM for 20 min
1282 and resuspended in Binding buffer (50mM NaH_2PO_4, pH 8.0 0.5 M NaCl). Cells were
1283 lysed using a French Press. Following lysing and centrifugation (15,000 RPM for 20
1284 min.) the lysate was added to a Ni-NTA column for binding, washing 4 times in buffer
1285 (Binding buffer with 20mM imidazole) and elution (binding buffer with 250 mM
1286 imidazole). Buffer exchange was performed in PBS. An SDS-PAGE gel was run to
1287 verify the size of the protein along with a ladder (Benchmark Protein Ladder).
1288
1289
1290 HIEM Generation
1291

1292 Human Intestinal Enteroid (HIEs) were cultured from 3D enteroid cultures derived from
1293 human colonic biopsy tissue using methods developed by Sato and Cleavers and 2-D
1294 enteroid monolayers (HEIMs) developed using methods of Van Dussen et al. (Sato *et*
1295 *al.*, 2009, 2011; VanDussen *et al.*, 2015; Saxena *et al.*, 2016). Briefly, HIEs were
1296 derived from human biopsy samples. The colonic crypts were isolated, embedded in
1297 Matrigel (Corning) or collagen (Sigma) and incubated with complete growth media with
1298 growth factors (CMGF+) for differentiation into 3D enteroid structures. Next, chambered
1299 slides (Greinier Bio-One) were coated with Matrigel or collagen, dissociated, about 50
1300 spheroids, (3D enteroids cultured $CMGF^{+}$ for 7 days) were added per well. HIEs were
1301 dissociated using 0.05% trypsin/0.5mM EDTA and a gravity flow strainer. Cells were
1302 allowed to grow and adhere 1-2 days with $CMGF^{-}$. Then the media was removed and
1303 replaced with Differentiation media. Typically for experiment, HEIMs were used 4-7
1304 days later when fully confluent (>90%) and differentiated. For our experiments this was
1305 day 5. The components of media the CMGF+, CMGF- and Differentiation media are
1306 described previously (Poole, Rajan and Maresso, 2018).
1307
1308 Glycan Microarray
1309 Glycan microarray analysis was performed by the Emory Comprehensive Glycomics
1310 Core using the methods described below.
1311
1312 An oligosaccharide array composed of 560 defined glycans from the Consortium for
1313 Functional Glycomics were obtained from MicroArray Core Facility of the Scripps
1314 Research Institute (La Jolla, CA) (lists can be found at

1315 http://www.functionalglycomics.org/static/consortium/resources/resourcecored2.shtml#
1316 Glycolipid) as described(Heimburg-Molinaro *et al.*, 2011). The glycans were printed on
1317 Nexterion 3-D hydrogel coating (H) slides using a contact printer in replicates of six. A
1318 second microarray consisting of 138 glycans from purified porcine gastric mucin was
1319 also included. And a third microarray consisted of 170 charged glycosaminoglycans
1320 (GAG), including oligomers from hyaluronic acid, chondroitin sulfates and heparan,
1321 obtained from the Emory Comprehensive Glycomics Core (Atlanta, GA). Glycans were
1322 conjugated with the bifunctional linker (AEAB) and printed on Nexterion 3-D hydrogel
1323 coated (H) slides using a contact printer Aushon 2470 (Quanterix, Billerica, MA) in
1324 replicates of four. His-tagged TFP (up to 40 ug/mL) was diluted in PBS buffer with 1%
1325 BSA and 0.05% Tween 20 and incubated on the microarray slides for 1 hr at RT. Slides
1326 were washed with PBS buffer with 0.05% Tween 20 and PBS buffer. Alexa Flour 647
1327 anti-His-tag mouse mAb (MBL International, Woburn, MA) was diluted to 5 µg/ml and
1328 incubated on the slides for 1 hr. After washing and drying, the slides were scanned with
1329 an InnoScan 1100 AL scanner and the data were processed using Mapix 8.2.5 software
1330 (Innopsys, Chicago, IL). Mean relative fluorescence units (RFU) from replicate spots
1331 were averaged after subtracting local median background, and the standard deviation
1332 (STDEV) were calculated and plotted as error bars in the histogram plot of the glycan
1333 array.

1334

1335 Bioinformatics modeling

1336

1337 The phage genome was annotated using the RASTtk (Brettin *et al.*, 2015). The Enzyme
1338 Function Initiative-Enzyme Similarity Tool (EFI-EST) was used to visualize BLAST
1339 results of the tail fiber protein (TFP) (Gerlt *et al.*, 2015). The network visualization
1340 showed that TFP was related to other tail fiber proteins and proteins that belong to the
1341 pectin lyase fold/virulence factor family of proteins (IPR011050). HHpred was used to
1342 identify other proteins with similar structures (Hildebrand *et al.*, 2009). The highest
1343 scoring template was a Tailspike protein from *E. coli* bacteriophage HK620 (PDB: 2VJJ;
1344 E-value = 9.4E-23). The other top five hits from Enterobacteria or *Escherichia* phages
1345 were a tailspike protein from Enterobacteria phage SF6 (PDB: 2VBK; E-value=1.9E-14),
1346 a putative endo-glycosidase tailspike protein (PDB: 6NW9; E-value=3.1E-14), a
1347 colanidase tailspike protein from Enterobacteria phage phi92 (PDB:6E0V; E-
1348 value=1.2E-13), a sugar-binding tailspike from *Salmonella* phage Det7 (PDB:6F7D; E-
1349 value=2.1E-12), and a K5 lyase (E.C.4.2.2.7) tailspike protein from Enterobacteria
1350 phage K5 (PDB: 2X3H; E-value=4E-12). All of these tailspike proteins bind and degrade
1351 polysaccharides and are classified as members of the pectin lyase fold/virulence factor
1352 family (IPR011050)(Freiberg *et al.*, 2003; Barbirz *et al.*, 2008; Schwarzer *et al.*, 2012;
1353 Broeker *et al.*, 2019; Greenfield *et al.*, 2019).The K5 lyase has well-known heparanase
1354 activity due to the similarities between K5 and heparan-sulfate (O'Leary, Xu and Liu,
1355 2013). All six were used to produce a predicted structure of the ES17 tail fiber protein in
1356 Modeler (Zimmermann *et al.*, 2018). Structures were aligned using UCSF Chimera.
1357 Chimera's matchmaker function was used to structurally align the predicted tail fiber 2
1358 protein with the HK620 tailspike and the K5 lyase. Solvent exposed identical residues
1359 between ES17 tail fiber protein 2 and K5 lyase were determined using Chimera's

1360 match-align to determine what residues were both identical and within 5 angstroms of
1361 each other in the structural alignment.
1362
1363 16S rRNA Gene Sequencing
1364
1365 The Center for Metagenomics and Microbiome Research (CMMR) at Baylor College of
1366 Medicine performed 16S rRNA sequencing and analysis.
1367
1368 The 16S rRNA gene sequencing methods were adapted from the methods developed for
1369 the Earth Microbiome Project (Caporaso *et al.*, 2012) and NIH-Human Microbiome Project
1370 (Caporaso *et al.*, 2012; Huttenhower *et al.*, 2012). Briefly, bacterial genomic DNA was
1371 extracted using the Qiagen MagAttract PowerSoil DNA Kit (formerly sold by MO BIO as
1372 PowerMag Soil DNA Isolation Kit). The 16S rDNA V4 region was amplified by PCR using
1373 primers 515F and 806R containing Illumina adapters and a single-index barcodes
1374 (Caporaso *et al.*, 2012). The amplicons were visualized with gel electrophoresis and
1375 purified to remove primer-dimers and non-specific amplicons. The samples were
1376 quantified using the Qubit® fluorometer and pooled at a DNA mass of 100 ng per sample.
1377 The amplicon pool was sequenced on the Illumina MiSeq platform using the reagent kit
1378 v2 (2 × 250 bp) and the paired-end protocol yielding paired-end reads that overlaped
1379 almost completely.
1380
1381 The raw data files in Binary Base Call (BCL) format created by the MiSeq run were first
1382 converted into the FASTQ format and demultiplexed based on the single-index barcodes

1383 using the Illumina BCL2FASTQ software. The demultiplexed FASTQ read pairs were then
1384 merged using USEARCH v7.0.1090 (Edgar, 2010) 'fastq_mergepairs' function, requiring
1385 read pairs to overlap by at least 50 bp, a merged length of at least 252 bp, a truncation
1386 quality above 5, and zero differences in the overlapping region. The merged files were
1387 then filtered further, using the USEARCH70 'fastq_filter' program, and only allowing for a
1388 maximum expected error of 0.05. Merged reads were then combined into a single FASTQ
1389 file, which was filtered for PhiX using Bowtie2 v.2.3.4.3 (Langmead and Salzberg, 2012)
1390 and the 'very-sensitive' parameter setting. After removing PhiX reads, the FASTQ file was
1391 transformed into a FASTA format file. The FASTA file was run through USEARCH70
1392 'derep_fulllength' program and the reads were sorted by size using usearch70 'sortbysize'
1393 program. The reads were clustered into operational taxonomic units (OTUs) at a similarity
1394 cutoff value of 97% using the UPARSE algorithm (Edgar, 2013). This was accomplished
1395 in an iterative stepwise manner in increments of 0.4% using USEARCH70 'cluster_otus'
1396 function. The output from the previous increment was fed into the next iteration, until a
1397 maximum of 3.2% was reached. All the intermediate files of this step were filtered for any
1398 chimeras and after the last run through the above loop, the final output was run through
1399 USEARCH70 'uchime_ref' program against the GOLD database (Kyrpides, 1999;
1400 Mukherjee *et al.*, 2019), using only the plus strand and allowing for no chimeras, in order
1401 to create a clustered OTU file with no chimeras. The OTU file was mapped against an
1402 optimized version of the latest current SILVA Database (Quast *et al.*, 2013) containing
1403 only sequences from the V4 region of the 16S rRNA gene to determine taxonomies. This
1404 step was performed using USEARCH70 'usearch_global' function, specifying the identity
1405 threshold to 96.8%. Abundances were recovered by mapping the demultiplexed reads to

1406 the OUT file and all files created in the loop were then run through a program developed
1407 in-house that resolved the iterative UPARSE steps, creating an OTU table in BIOM format
1408 and removing the chimera and singleton reads. The BIOM file was summarized, recording
1409 the number of reads per sample, and merged with a file that was generated for the overall
1410 read statistics, to produce a final summary file with read statistics and taxonomy
1411 information. ATIMA (Agile Toolkit for Incisive Microbial Analyses) was used to generate
1412 beta diversity graphs.
1413
1414 **Supplemental References**
1415
1416 Barbirz, S. *et al.* (2008). Crystal structure of *Escherichia coli* phage HK620 tailspike:
1417 podoviral tailspike endoglycosidase modules are evolutionarily related. Mol. Microbiol.
1418 *2*, 303–316.
1419
1420 Brettin, T. *et al.* (2015). RASTtk: a modular and extensible implementation of the RAST
1421 algorithm for building custom annotation pipelines and annotating batches of genomes.
1422 Sci. Rep.*5*, 8365.
1423
1424 Broeker, N. K. *et al.* (2019). Time-resolved DNA release from an O-antigen-specific. J.
1425 Biol. Chem. *31*, 11751–11761.
1426
1427 Caporaso, J. G. *et al.* (2012). Ultra-high-throughput microbial community analysis on the
1428 Illumina HiSeq and MiSeq platforms, ISME J. doi: 10.1038/ismej.2012.8.

1429

1430 Edgar, R. C. (2010). Search and clustering orders of magnitude faster than BLAST',
1431 Bioinformatics. doi: 10.1093/bioinformatics/btq461.

1432

1433 Edgar, R. C. (2013). UPARSE: Highly accurate OTU sequences from microbial
1434 amplicon reads. Nat. Methods. doi: 10.1038/nmeth.2604.

1435

1436 Freiberg, A. *et al.* (2003). The tailspike protein of Shigella phage Sf6. A structural
1437 homolog of Salmonella phage P22 tailspike protein without sequence similarity in the
1438 beta-helix domain. J. Biol. Chem. *3*, 1542–1548.

1439

1440 Gerlt, J. A. *et al.* (2015). Enzyme Function Initiative-Enzyme Similarity Tool (EFI-EST):
1441 A web tool for generating protein sequence similarity networks. Biochim. Biophys. Acta.
1442 *8*,1019–1037.

1443

1444 Greenfield, J. *et al.* (2019). Structure and tailspike glycosidase machinery of ORF212
1445 from E. coli O157:H7 phage CBA120 (TSP3). Sci. Rep.*1*, 7349.

1446

1447 Heimburg-Molinaro, J. *et al.* (2011). Preparation and analysis of glycan microarrays.
1448 Curr. Protoc. Protein. Sci. doi: 10.1002/0471140864.ps1210s64.

1449

1450 Hildebrand, A. *et al.* (2009). Fast and accurate automatic structure prediction with
1451 HHpred. Proteins. *9*, 128–132.

1452

1453 Huttenhower, C. *et al.* (2012). Structure, function and diversity of the healthy human
1454 microbiome. Nature. doi: 10.1038/nature11234.

1455

1456 Kyrpides, N. C. (1999). Genomes Online Database (GOLD 1.0): A monitor of complete
1457 and ongoing genome projects world-wide. Bioinformatics. doi:
1458 10.1093/bioinformatics/15.9.773.

1459

1460 Langmead, B. and Salzberg, S. L. (2012). Fast gapped-read alignment with Bowtie 2',
1461 Nat. Methods. doi: 10.1038/nmeth.1923.

1462

1463 De Lisle, R. C., Roach, E. and Jansson, K. (2007). Effects of laxative and N-
1464 acetylcysteine on mucus accumulation, bacterial load, transit, and inflammation in the
1465 cystic fibrosis mouse small intestine. Am. J. Physiol. Gastrointest. Liver Physiol. doi:
1466 10.1152/ajpgi.00195.2007.

1467

1468 Mukherjee, S. *et al.* (2019). Genomes OnLine database (GOLD) v.7: Updates and new
1469 features. Nucleic. Acids Res. Publ. doi: 10.1093/nar/gky977.

1470 O'Leary, T. R., Xu, Y. and Liu, J. (2013) 'Investigation of the substrate specificity of K5
1471 lyase A from K5A bacteriophage. Glycobiology. *1*, 132–141.

1472

1473 Poole, N. M., Rajan, A. and Maresso, A. W. (2018). Human Intestinal Enteroids for the
1474 Study of Bacterial Adherence, Invasion, and Translocation. Curr. Protoc. Microbiol. *1*,

1475 e55.

1476

1477 Quast, C. *et al.* (2013). The SILVA ribosomal RNA gene database project: Improved
1478 data processing and web-based tools. Nucleic Acids Res. Spec. Publ. doi:
1479 10.1093/nar/gks1219.

1480

1481 Sato, T. *et al.* (2009). Single Lgr5 stem cells build crypt-villus structures in vitro without
1482 a mesenchymal niche. Nature. doi: 10.1038/nature07935.

1483

1484 Sato, T. *et al.* (2011). Long-term expansion of epithelial organoids from human colon,
1485 adenoma, adenocarcinoma, and Barrett's epithelium. Gastroenterology. doi:
1486 10.1053/j.gastro.2011.07.050.

1487

1488 Saxena, K. *et al.* (2016). Human Intestinal Enteroids: a New Model To Study Human
1489 Rotavirus Infection, Host Restriction, and Pathophysiology. J. Virol.*1*,43–56.

1490

1491 Schwarzer, D. *et al.* (2012). A multivalent adsorption apparatus explains the broad host
1492 range of phage phi92: a comprehensive genomic and structural analysis. J. Virol.*19*,
1493 10384–10398.

1494

1495 VanDussen, K. L. *et al.* (2015). Development of an enhanced human gastrointestinal
1496 epithelial culture system to facilitate patient-based assays. Gut. doi: 10.1136/gutjnl-
1497 2013-306651.

Wintersinger, J. A. and Wasmuth, J. D. (2015). Kablammo: An interactive, web-based BLAST results visualizer. Bioinformatics. doi: 10.1093/bioinformatics/btu808.

Zimmermann, L. *et al.* (2018). A Completely Reimplemented MPI Bioinformatics Toolkit with a New HHpred Server at its Core. J. Mol. Biol. *15*, 2237–2243.